Materials Analysis and Modeling of Underfill Materials

Nicholas B. Wyatt and Robert S. Chambers

Sandia National Laboratories

Materials Analysis and Modeling of Underfill Materials

Nicholas B. Wyatt[1] and Robert S. Chambers[2]
[1]Organic Materials Science
[2]Component Science and Mechanics
Sandia National Laboratories
P.O. Box 5800
Albuquerque, New Mexico 87185-MS0958

Abstract

The thermal-mechanical properties of three potential underfill candidate materials for PBGA applications are characterized and reported. Two of the materials are a formulations developed at Sandia for underfill applications while the third is a commercial product that utilizes a snap-cure chemistry to drastically reduce cure time. Viscoelastic models were calibrated and fit using the property data collected for one of the Sandia formulated materials. Along with the thermal-mechanical analyses performed, a series of simple bi-material strip tests were conducted to comparatively analyze the relative effects of cure and thermal shrinkage amongst the materials under consideration. Finally, current knowledge gaps as well as questions arising from the present study are identified and a path forward presented.

ACKNOWLEDGMENTS

CONTENTS

FIGURES

TABLES

NOMENCLATURE

CTE	Coefficient of Thermal Expansion
DMA	Dynamic Mechanical Analysis
DSC	Differential Scanning Calorimetry
NSC	National Security Campus
PBGA	Plastic Ball Grid Array
PCB	Printed Circuit Board
PEC	Potential Energy Clock Model
SPEC	Simplified Potential Energy Clock Model
T_g	Glass Transition Temperature
TMA	Thermo-Mechanical Analysis
WLF	Williams-Landel-Ferry Equation

1. INTRODUCTION

In modern electronics packaging schemes, adhesive underfills are often used to improve the lifetime performance of components such as plastic ball grid arrays (PBGA's) on printed circuit boards (Figure 1). This underfill adhesive provides a stronger mechanical connection and distributes the stress generated from thermal expansion mismatches between the component and circuit board thereby reducing stress concentrations in the solder joints. Due to production demands and desires to speed up processing and throughput, the electronics industry has moved away from traditional encapsulants (e.g., epoxy-amine based systems) in favor of snap-cure chemistries.[1] These snap-cure materials are attractive due to their low flow times (low viscosity) and very short curing times (typically on the order of minutes). However, questions remain about the cure shrinkage stresses generated by the snap cured material when cured in these highly confined environments.
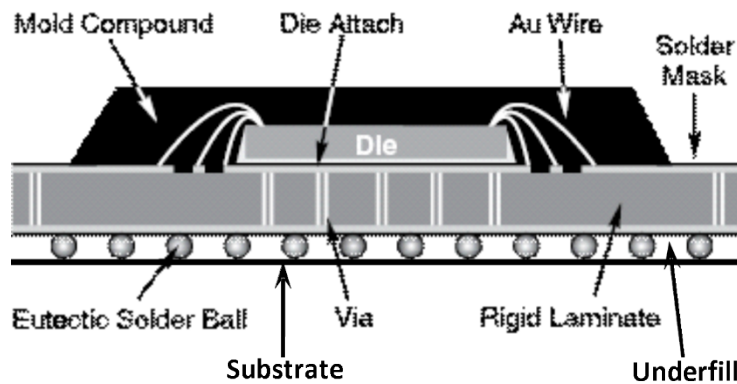
Figure 1. Schematic representation of a PBGA with underfill

The purpose of this report is to document the thermal-mechanical analyses, cure analyses, and associated material modeling that was undertaken to further understand the viscoelastic and stress behavior of three underfill candidate materials. The materials analyzed were Zymet X2821 (a commercial snap-cure underfill product) and a Sandia formulated mixture of EPON 828 cured with Jeffamine D230 filled at two different volumetric loadings of aluminum oxide (20 and 30 volume percent, Almatis A20 SG alumina in these studies). Of particular interest to PBGA applications was understanding the relative contributions of cure and thermal shrinkage to stress generated in the very confined environment beneath a PBGA. Thus, tests were developed that allowed a relative comparison of the contributions of cure shrinkage and thermal contraction to the overall stress state among the various materials studied.

2. THERMAL-MECHANICAL ANALYSES

Before attempts could be made to understand the cure and thermal stresses generated by the various materials of interest, a suite of thermal-mechanical tests were performed to increase understanding of the basic material properties. These material properties were and can be used to inform and parameterize predictive models to better understand the viscoelastic behavior of the materials in various configurations and environments. In this section we give a summary of the testing that was performed and data gathered for three underfill materials: Zymet X2821, EPON 828/D230/30vol% alumina, and EPON 828/D230/20 vol% alumina.

2.1 Zymet X2821

Zymet X2821 is a commercial underfill material produced by Zymet Inc. (East Hanover, NJ, USA). The chemical makeup of this material was recently studied by Celina et al. and summarized in a SAND report.[2] In part, they found that the chemical constituents of this material include an epoxidized cyclohexyl ester along with a hydroxyl-oxetane and a bis-oxetane material. Further, the material incorporates approximately 49% by weight inorganic silica filler, presumably to reduce the overall CTE of the cured underfill.

2.1.1 Cure and Exotherm Considerations

Zymet X2821, like other snap-cure materials, is characterized by a very fast cure reaction that occurs at relatively high temperatures. In the case of Zymet X2821, the manufacturer suggests a cure time of just 10 minutes at 120 °C. Given this recommendation and the nature of snap-cure materials, the chemical reaction was assumed to be extremely exothermic. This assumption was verified by differential scanning calorimetry (DSC) measurements on the cure of Zymet under the recommended conditions (Figure 2). For this test, a small sample of Zymet X2821 (21.09 mg) was put into the DSC chamber at room temperature. The sample was heated to 120 °C at 20 °C/min, and then held at 120 °C for 10 minutes.
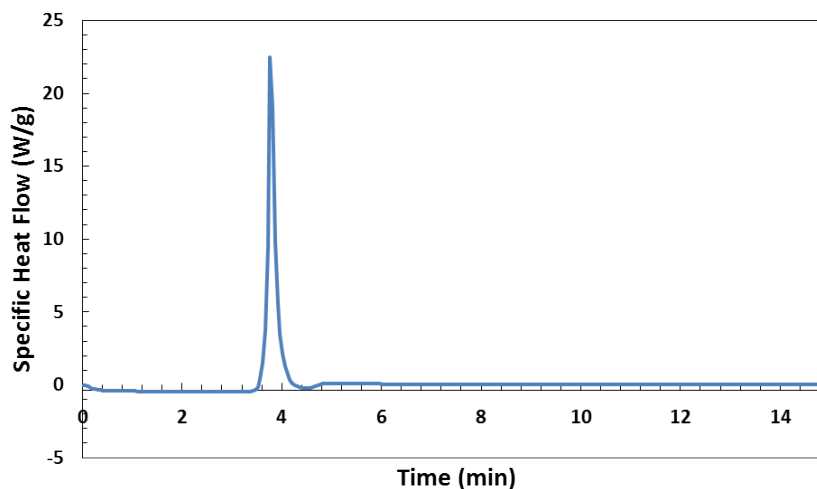
Figure 2. Specific heat flow for Zymet X2821 during cure (exotherm up)

DSC results confirm a very large, sharp reaction exotherm and verify that the material is fully cured after 10 minutes at 120 °C. Further, the reaction exotherm occurs before the sample attained 120 °C, beginning at approximately 100 °C and finishing by approximately 115 °C. However, it is important to note that the temperatures reported are the temperatures in the DSC chamber and not necessarily the sample temperature. Thus, the large exotherm observed in the DSC measurement led to concerns about the accompanying temperature rise to which parts could be subjected in the vicinity of the Zymet material. Therefore, a series of tests were performed to measure the temperature rise in the bulk material in different geometries to analyze the temperature rise (Figure 3). These tests were done by placing a prescribed amount of underfill material (0.045 – 2.0 g) into a cylindrical container, placing a thermocouple in the center of the bulk material, then placing the setup into a 120 °C oven. The temperature was then monitored for 10 minutes, corresponding to the recommended 10 minute cure time.
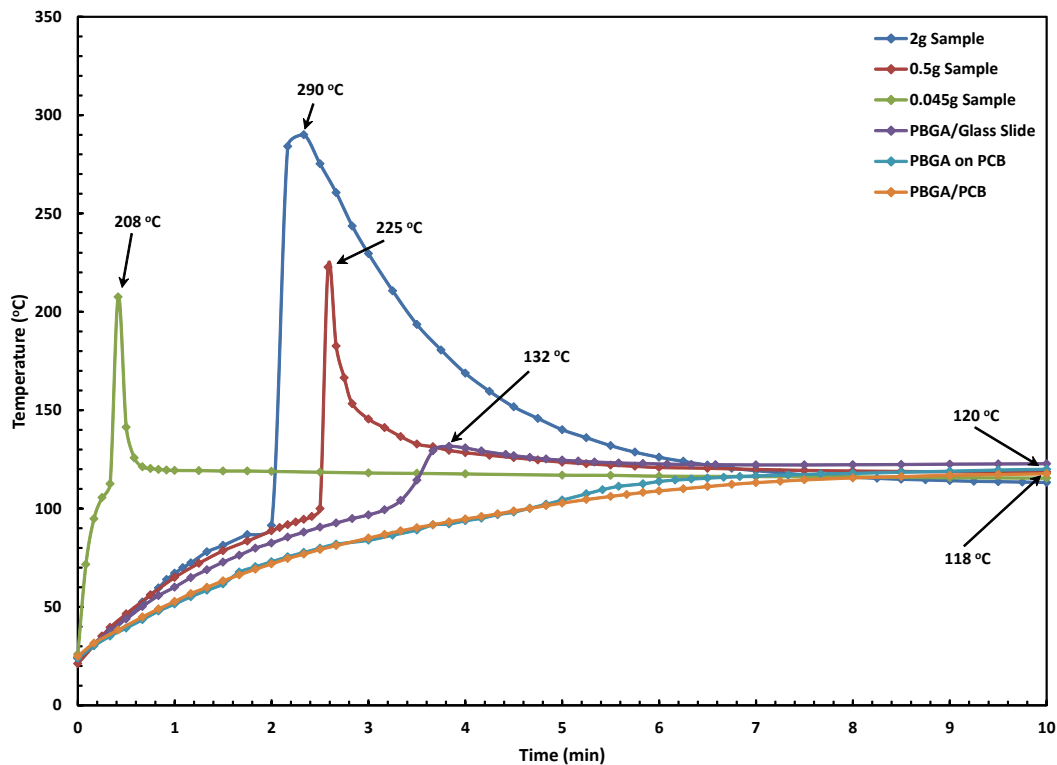
Figure 3. Exothermic temperature rise for various masses of Zymet X2821 during cure

The first three tests were done in aluminum pans of varying diameter. Results from the smallest mass of Zymet X2821 (0.045 g) in an aluminum DSC pan showed a maximum bulk material temperature of 208 °C, which would be unacceptable for a printed circuit board. Due to this extreme temperature rise, follow-on testing was performed to determine if the underfill material beneath a PBGA showed similar results. For the first of these follow-on tests, a 400 ball, 1.25 mm pitch PBGA was staked to a glass microscope slide. A fine gauge thermocouple was then fed into the space beneath the PBGA with the measuring end at the center of the package. The PBGA was then underfilled and cured as described above while monitoring the temperature. In this case, the maximum temperature observed was only 132 °C. Finally, the test was repeated

14

with a PBGA staked to a printed circuit board (PCB) with a thermocouple beneath. These tests showed maximum temperatures of 120 °C and 118 °C. These tests show that the thin bondline and high surface area beneath the PBGA on a printed circuit board are sufficient to quickly diffuse the heat generated from the exothermic cure and mitigate any potential extreme temperature excursion for the package. Duplicate tests performed by collaborators at NSC showed similar results.

2.1.2 Dynamic Modulus

For this and subsequently described thermal-analysis tests a sample of Zymet X2821 was cured in a plaque mold consisting of two ¼" thick stainless steel plates separated by a 2 mm spacer. The sample was then cut to the appropriate shape and dimensions for the testing described.

The dynamic storage and loss moduli (E' and E", respectively) were measured on a rectangular material sample (17.22mm X 5.69mm X 1.52 mm) in a single cantilever geometry in a TA Instruments Q800 DMA. In this setup, one end of the sample is clamped while an oscillatory strain is applied to the opposite end. For the testing reported here, the frequency of the oscillation was 1.0 Hz and had a strain amplitude of 0.1 %. First, the sample was equilibrated at 0 °C, then the oscillation was applied while the temperature was increased to 275 °C at a rate of 2 °C/min (Figure 4).
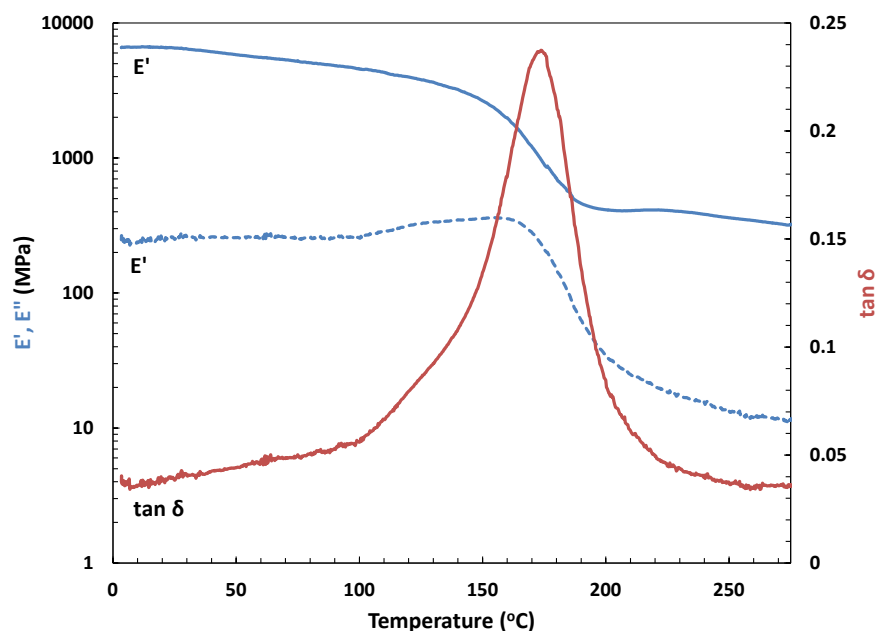
Figure 4. Dynamic moduli as a function of temperature for Zymet X2821

The results show a glassy modulus (E' for T < 100 °C) for Zymet X2821 that is on the order of that expected for similarly filled thermoset materials. The glass transition temperature (T_g), defined by the peak in the tan δ curve is approximately 175 °C for the fully cured material. Also of note is the relatively small difference between the glassy and rubbery moduli (approximately 6 GPa and 0.3 GPa, respectively). Typical thermoset materials show a larger difference between these moduli, usually on the order to 1.5 to 2 orders of magnitude (or more). This relatively

15

smaller change is likely due to the network structure created by the unique chemistry and cross-linking behavior of this snap-cure material.

2.1.3 Shear Modulus

The shear modulus is measured in a manner similar to that used for the dynamic moduli, but the sample is subjected to a torsional deformation rather than a flexural/bending deformation. Here, a rectangular sample (31.85 mm X 12.09 mm X 1.54 mm) was torsionally oscillated at one end at a frequency of 1.0 Hz with a strain amplitude of 0.5% while measuring the response at the opposite end in a TA Instruments ARES rheometer. During this oscillation the temperature was ramped from 25 °C to 250 °C at a rate of 2 °C/min to measure the temperature dependence of the shear moduli (Figure 5).
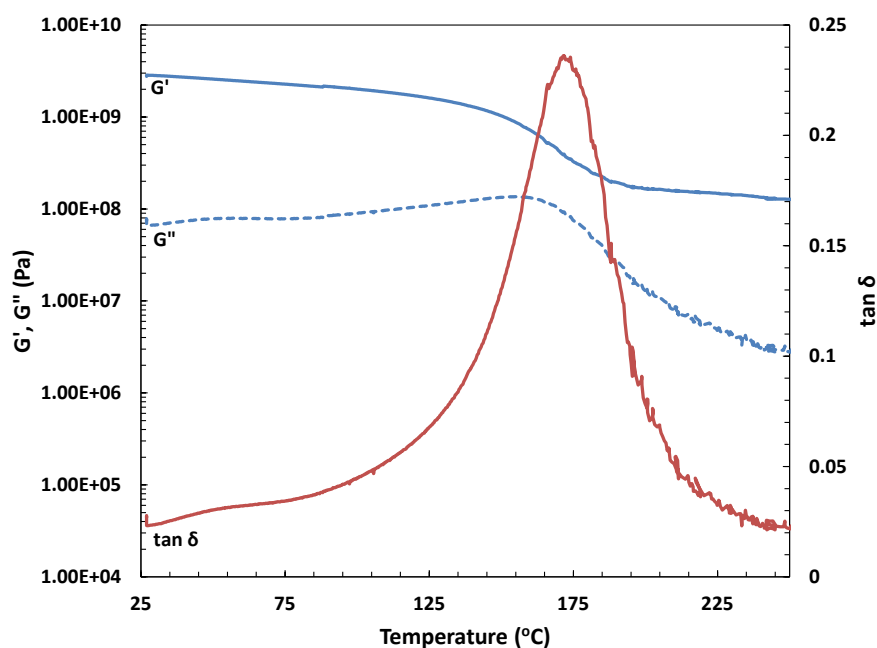
Figure 5. Temperature dependence of the shear moduli for Zymet X2821

The glass transition temperature, again defined by the peak in the tan δ curve, is approximately 170 °C. Also, similar to the dynamic moduli results, the difference in magnitude between the glassy and rubbery shear modulus is lower than what is typically observed for thermoset materials and is likely due to differences in network structure and the presence of an inorganic filler.

2.1.4 Time Temperature Superposition

The principle of time-temperature superposition with respect to polymer materials allows measurements taken across a broad range of temperatures to be shifted relative to a reference temperature to obtain a master curve. This allows the observation of frequency or time dependent behavior at a particular temperature over a much larger range of time scales than would be experimentally feasible. Shifting the resulting master curve to a particular temperature

of interest then allows the prediction of the material behavior at that temperature. For the purposes of these studies, the master curve is generated by measuring the frequency dependent response of the shear moduli at many temperatures, then shifting the resulting curves relative to a reference temperature to create a single curve covering many orders of magnitude in frequency. These results can then be converted into the time domain to predict the time dependent relaxation behavior of the material at a given temperature.

Similar to the shear modulus measurements described in Section 2.1.3, these measurements were taken on a single rectangular sample (31.85 mm X 12.10 mm X 1.57 mm) by oscillating torsionally with a strain amplitude of 0.5% while varying the frequency from 0.01 to 20 Hz. The sample was heated to the highest temperature (120 °C) and allowed to equilibrate for at least 15 minutes before the first measurement. Following each set of measurements at a given temperature, the temperature was decreased by 5 °C. The sample was then allowed to equilibrate for 10 minutes before proceeding with the next set of measurements. Once the measurements were completed at all of the desired temperatures from 120 °C to 75 °C a reference temperature (T_{ref}) of 175 °C was chosen and each data set was shifted (i.e., frequency was multiplied by a constant value a_T) along the horizontal axis to align the curve with those surrounding it (Figure 6). Note that the shift factors in this case were based solely on the tan δ curves and that no vertical shifting of the data was employed.
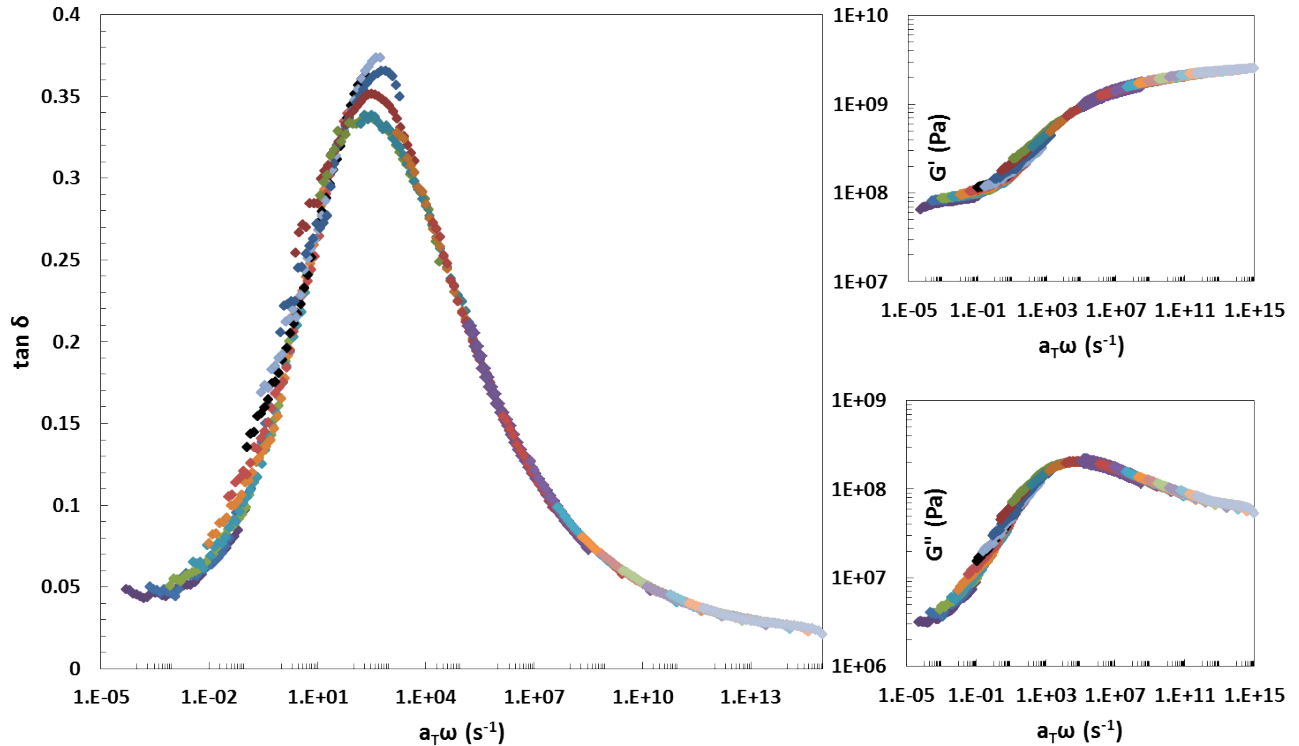
Figure 6. Time-temperature superposition results for Zymet X2821 with T_{ref} = 175 °C

Once the data have been satisfactorily shifted, the shift factors can be plotted against the temperature associated with it on a semi-log plot and then fit with the Williams-Landel-Ferry (WLF) equation (Equation 1) to allow the estimation of shift factors outside of the temperature range measured here.

$$\log(a_T) = \frac{-C_1(T - T_{ref})}{C_2 + (T - T_{ref})}$$

(1)

The results of the WLF fit, with the expected departure from WLF behavior below Tg, are shown in Figure 7. For this fit, $C_1 = 17.8$ and $C_2 = 181.0$.
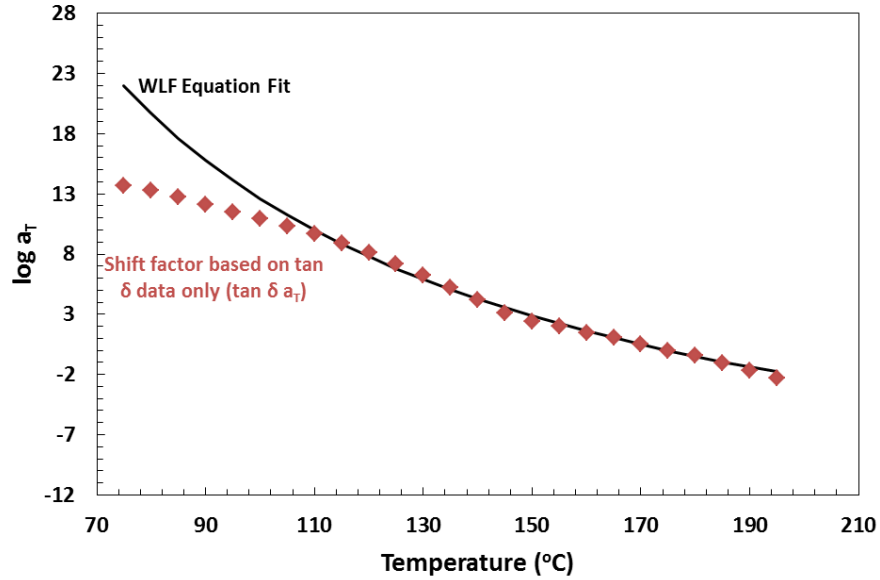
Figure 7. WLF fit of the TTS shift factors for Zymet X2821

2.1.5 Thermal Expansion

The thermal expansion of Zymet X2821 was measured using a TA Instruments Q400 TMA with a quartz expansion probe. For this test, a test sample is placed on a platform within an environmental chamber. A probe is then placed in light contact with the top surface of the test sample. The height of the sample is then continuously measured as the temperature changes. Since the original sample height is known, thermal strain can be calculated from the measured change in height (Figure 8). The coefficient of thermal expansion (CTE) is calculated as the slope of the dimension change versus temperature curve and is also shown in Figure 8.

18
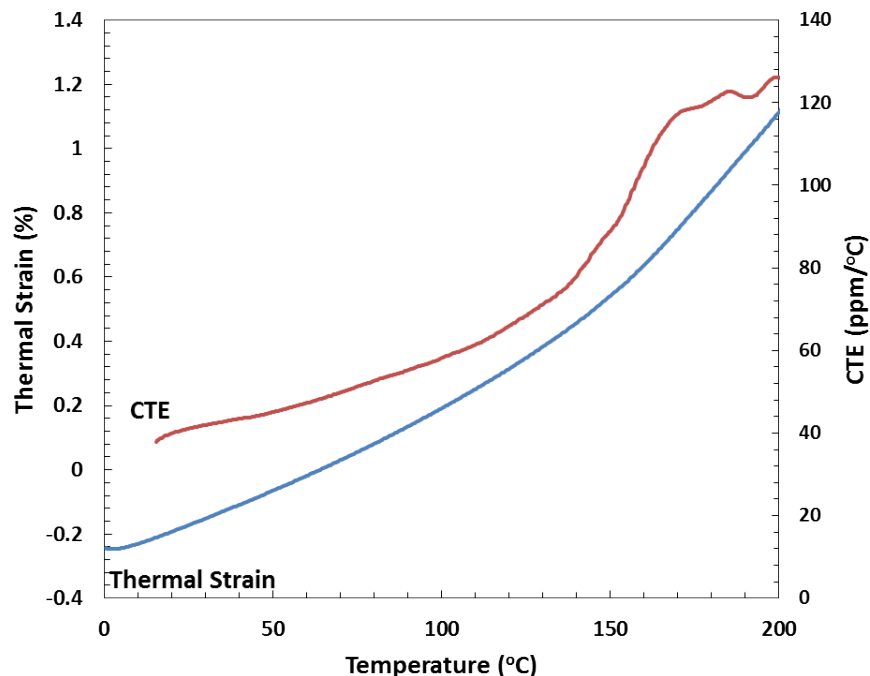
Figure 8. Thermal strain and CTE as a function of temperature for Zymet X2821

The results from the thermomechanical analysis test give a room temperature glassy CTE of approximately 40 ppm/°C and a rubbery CTE of approximately 120 ppm/°C. Further, the T_g determined from these results is about 160 °C, which is reasonably consistent with the T_g determined from the shear and dynamic moduli measurements.

2.1.6 Compression

The final characterization testing that was done for Zymet X2821 was compression testing. For these tests, cylinders of the cured material having an aspect ratio of 2:1 (height = 9.9 mm, diameter = 4.6 mm) were annealed at 120 °C for 15 minutes and then cooled to room temperature at a rate of 2 °C/min. The samples were allowed to equilibrate at the test temperature for approximately 1 hour prior to testing. Four different temperatures ranging from -55 °C to 50 °C were tested. For the compression test, the sample was compressed at a rate of 0.05 inches/min in an Instron load frame until yield was observed. From the resulting load-displacement data a compressive stress versus strain plot can be calculated. Representative data for each temperature tested are shown in Figure 9.
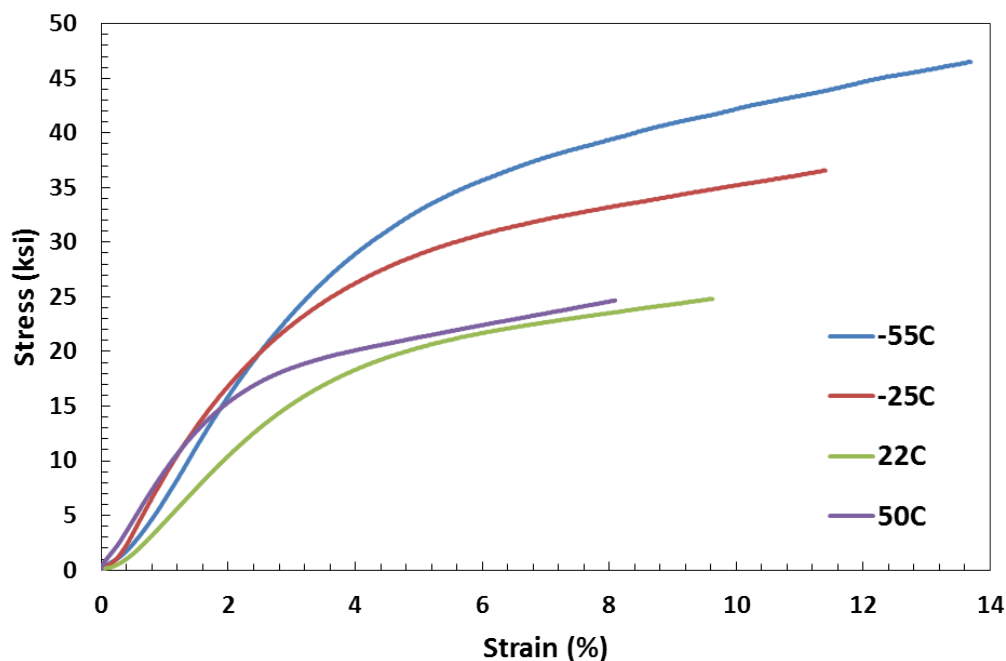
Figure 9. Compressive stress versus strain at various temperatures for Zymet X2821

A compressive modulus can be calculated from the compressive stress versus strain curves generated from these tests. The modulus is calculated as the slope of the stress versus strain curve at low strain values. The moduli reported in Table 1 are the averages of three independent measurements on separate samples at each temperature. Note that there is relatively little change in the modulus over the temperature range spanning from -55 °C to 50 °C. This trend is not surprising as all of these measurements occurred well below T_g so the material is well into the glassy state in each case.

Table 1. Compressive modulus at various temperatures for Zymet X2821

Temperature (°C)	Compressive Modulus* (ksi)	Standard Deviation
-55	576	25
-25	593	72
22	594	56
50	505	35

*average of 3 independent measurements

2.2 EPON828/D230/30vol% Alumina

The resin system consisting of EPON 828 cured with Jeffamine D230 and filled with alumina was developed at Sandia as a replacement underfill material for one that is no longer commercially available. As developed, there are provisions for three different volumetric loadings of the alumina filler: 20, 30, and 40 percent with the 30 percent filler fraction being the most commonly used. This system is cured in a two stage process. It is first cured for one hour

at 50 ºC followed by a three hour cure at 80 ºC. These relatively mild cure temperatures are considered to be acceptable for electronic components and printed wiring assemblies and adverse effects to the assembly due to the thermal exposure are not expected.

2.2.1 Dynamic Modulus

As with the Zymet material described above, the thermal-mechanical properties of the EPON 828/D230/30vol% alumina system were measured. Using a single cantilever test geometry and a rectangular material sample (17.04 mm X 6.19 mm X 1.56 mm), the dynamic moduli were measured (using an oscillation at 1 Hz and 0.1% strain) as a function of temperature over a range of temperatures spanning from 30 ºC to 140 ºC at a ramp rate of 1 ºC/min (Figure 10). At room temperature, the glassy modulus of this system is slightly lower than that of the Zymet X2821 material. Further, the glass transition temperature, defined by the peak in the tan δ curve, is about 95 ºC (compared to 175 ºC for Zymet X2821).
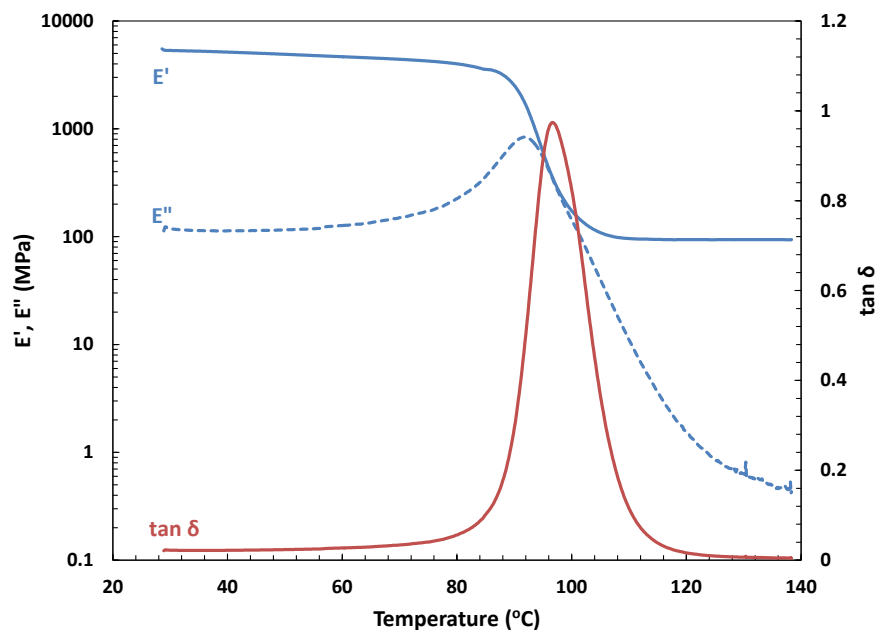
Figure 10. Temperature dependence of the dynamic moduli for EPON 828/D230/30Vol% Alumina

2.2.2 Shear Modulus

The shear modulus was also measured for the EPON 828/D230/30vol% alumina system using a rectangular torsion sample having dimensions 8.61mm X 2.26 mm X 31.62 mm. These measurements were done while oscillating at 1Hz and either 0.01% or 0.1% strain (Figure 11). The temperature was ramped from 25 ºC to 150 ºC at a rate of 1 ºC/min. As a check for consistency, the test was also run at a temperature ramp rate of 0.5 ºC/min with very good agreement between the two sets of measurements. This agreement suggests that thermal lag between the environmental chamber and the sample was negligible.

21
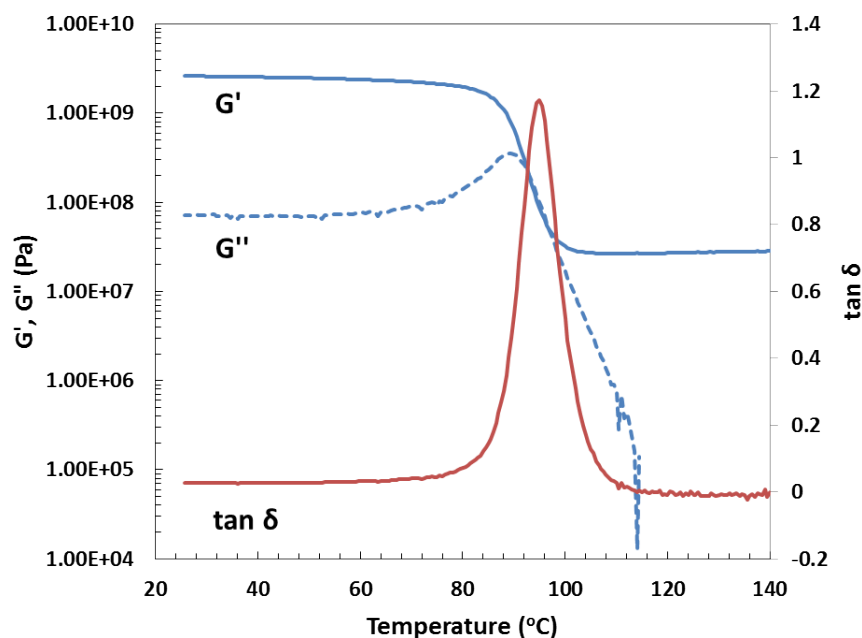
Figure 11. Shear moduli as a function of temperature for EPON 828/D230/30Vol% Alumina

2.2.3 Master Curve

Following the procedure outlined in Section 2.1.4 , the frequency dependent response of the 30 vol% filled material was probed over a range of temperatures spanning from 50 °C to 120 °C using a rectangular sample (31.62 mm X 8.61 mm X 2.26 mm). For these measurements, the sample was first heated to the highest temperature (120 °C), allowed to equilibrate for about 30 minutes, then oscillated with a strain of 0.1% while varying the frequency from 0.01 Hz to 20 Hz. The temperature was then changed by 5-10 °C and the sample allowed to equilibrate for 10 minutes before repeating the measurement. Strain sweep measurements at the extremes of the temperature range tested confirmed that the chosen strain of 0.1% was well within the linear viscoelastic regime for this material. Following the measurements, the frequency dependent data were shifted relative to a reference temperature of 90 °C to obtain a master curve in the frequency domain (Figure 12). Note that the shifting was done relative to the tan δ curve only and that no vertical shifting was done.
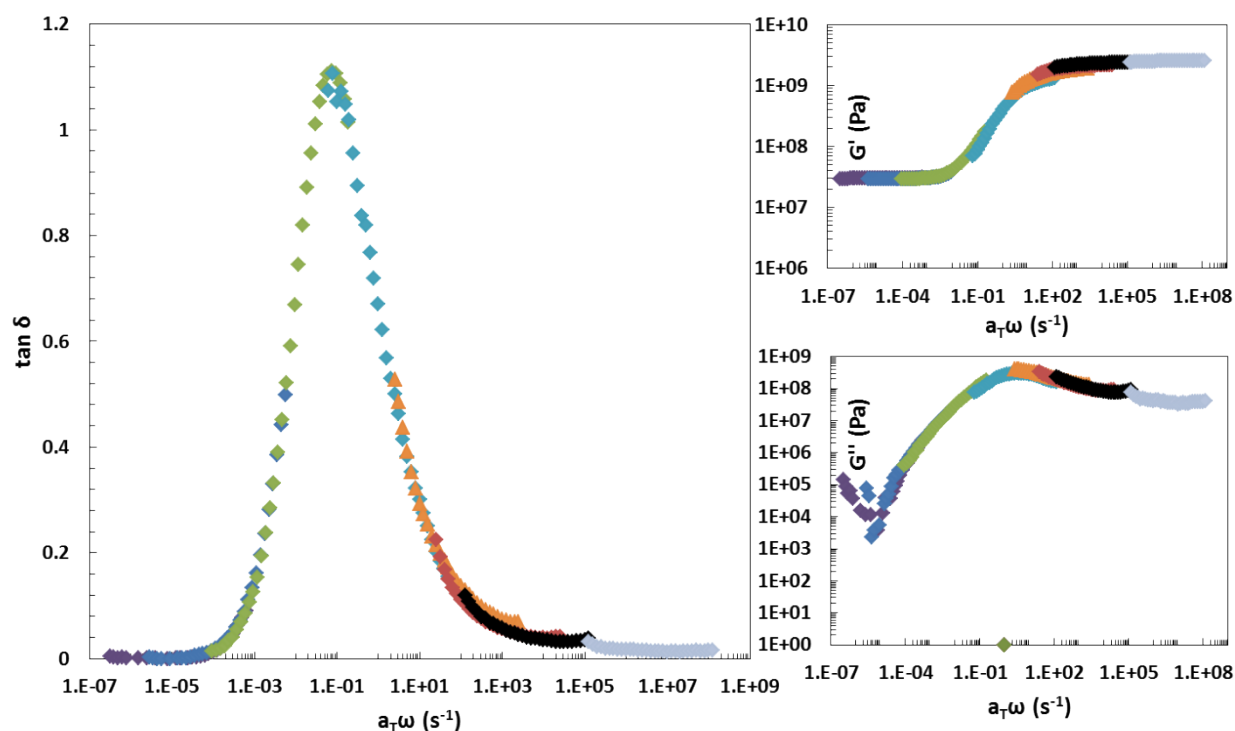
Figure 12. Time-temperature superposition results for EPON 828/D230/30vol% Alumina with T_{ref} = 90 °C

The shift factors associated with the time-temperature superposition shown in Figure 12 were then fit using the WLF equation (Equation 1) with the expected departure from WLF behavior below the glass transition behavior (Figure 13) yielding constants C_1 = 11.6 and C_2 = 36.5 for a reference temperature of 90 °C. Note that choosing a different reference temperature and employing vertical shifts in the data to account for non-equilibrium effects will result in different fitting parameters in the WLF equation.
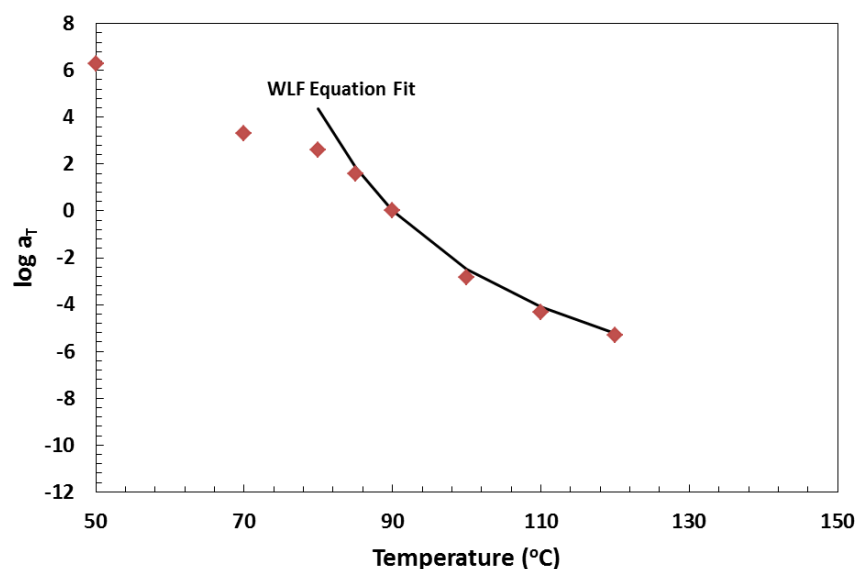
Figure 13. WLF equation fit to the TTS shift factors for EPON 828/D230/30vol% Alumina

2.2.4 Thermal Expansion

The thermal expansion behavior of the EPON 828/D230/30vol% alumina system was also probed using the thermo-mechanical analysis techniques described in Section 2.1.5. For these measurements, a rectangular sample of 4.30mm X 4.02 mm X 8.74 mm was placed on a testing surface with a quartz probe in light contact with the top surface. The height of the sample was measured as a function of temperature over the range 0 °C to 150 °C while ramping the temperature at a rate of 2 °C/min. The results give a measure of both the coefficient of thermal expansion (CTE) and the thermal strain as a function of temperature Figure 14. The glassy and rubbery CTE for this material are approximately 30-40 ppm/°C and 135 ppm/°C, respectively. While the glassy CTE is very similar to that of Zymet X2821, the rubbery CTE of Zymet is slightly lower (120 ppm/°C). The T_g determined from these measurements for EPON828/D230/30vol% alumina is 85 °C which agrees reasonably well with that obtained from other measurements.

24
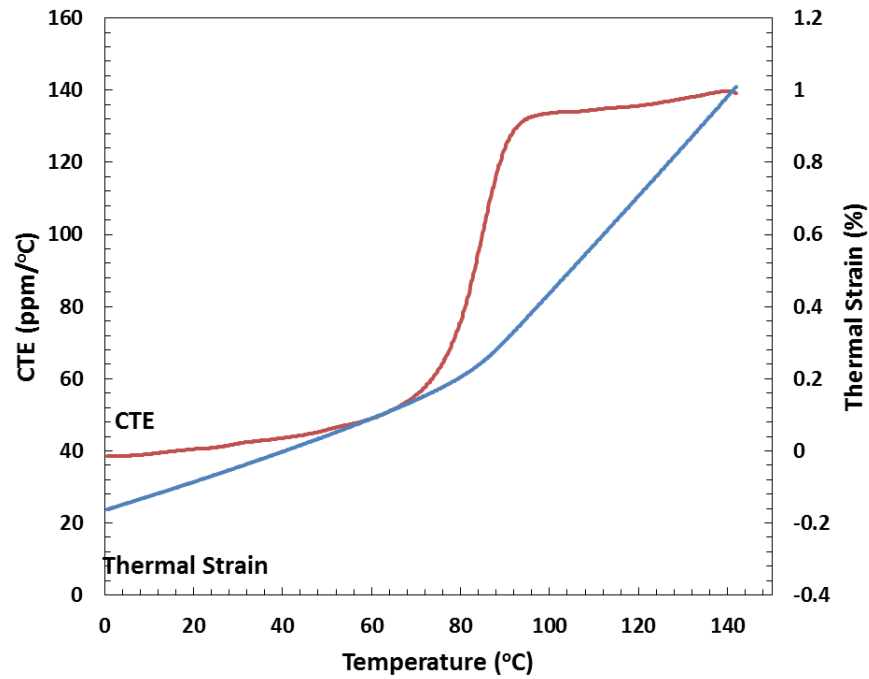
Figure 14. Thermal strain and CTE as a function of temperature for EPON 828/D230/30vol% alumina

2.2.5 Compression

Lastly, the compression response of EPON828/D230/30vol% alumina was measured. For compression tests, cylindrical samples having diameter 8.5 mm and height of 18 mm were fabricated, then annealed at 100 ºC for 15 minutes. Following the high temperature anneal, the samples were cooled to room temperature at approximately 2 ºC/min. The samples were then compressed at a rate of 0.05 in/min at -55 ºC, -25 ºC, 22 ºC, or 50 ºC following a minimum of 1 hour at temperature for equilibration. Four samples were tested at each temperature and representative stress versus strain curves for each temperature are given in Figure 15.
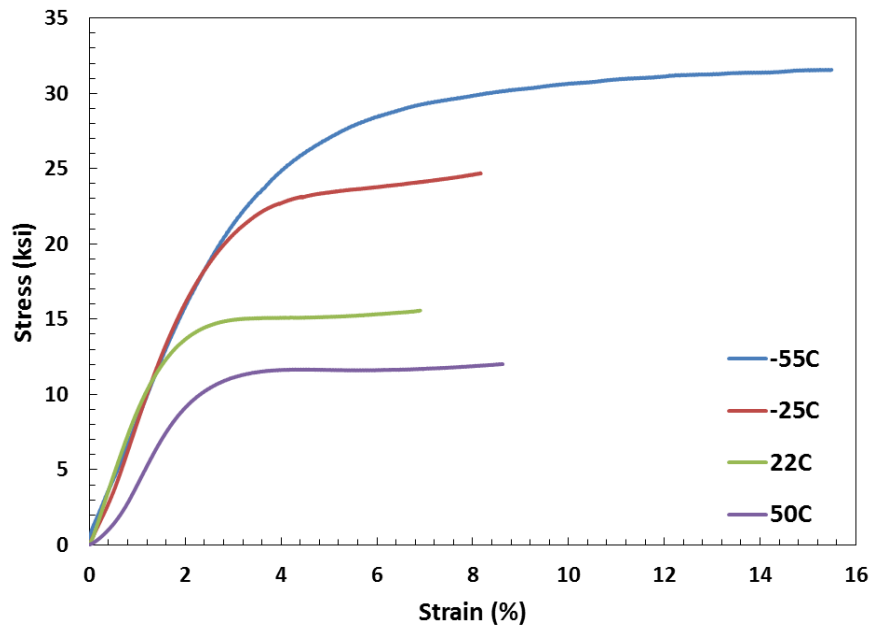
Figure 15. Compressive stress versus strain for EPON828/D230/30vol% alumina at several temperatures

A compressive modulus was calculated from the compressive stress versus strain curves generated from these tests. The moduli reported in Table 2 are the averages of four independent measurements on separate samples at each temperature. Note that, as with Zymet X2821, there is relatively little change in the modulus over the temperature range spanning from -55 °C to 50 °C.

Table 2. Compressive modulus at various temperatures for EPON828/D230/30vol% alumina

Temperature (ºC)	Compressive Modulus* (ksi)	Standard Deviation
-55	558	31
-25	533	25
22	559	12
50	512	49

*average of 4 independent measurements

2.3 EPON828/D230/20vol% Alumina

One of the important properties influencing the usability of an underfill material is its viscosity. Underfill materials are required to flow in the highly confined space beneath an electronic package. As such, a low viscosity is advantageous as the higher the viscosity, the more resistance to flow exists. Since fillers tend to raise the viscosity of a formulation, it was deemed appropriate to investigate and characterize that EPON828/D230 material at a lower filler

26

fraction. As such, the 20 vol% filler fraction material was selected and analyzed as described above. The measurement details for this material closely follow those detailed above, and so will be omitted in this section for brevity. Notable exceptions to testing procedures or the resulting data are discussed below.

2.3.1 Dynamic Modulus

The dynamic moduli were measured using a TA Instruments RSAG2 DMA in a single cantilever geometry. The rectangular sample dimensions for this test were 41.31 mm X 9.36 mm X 1.97 mm. The temperature was increased from 25 °C to 140 °C at a rate of 1 °C/min while oscillating at a frequency of 1 Hz and strain amplitude of 0.1% (Figure 16). The T_g, taken as the peak in the tan δ curve, is 90 °C.
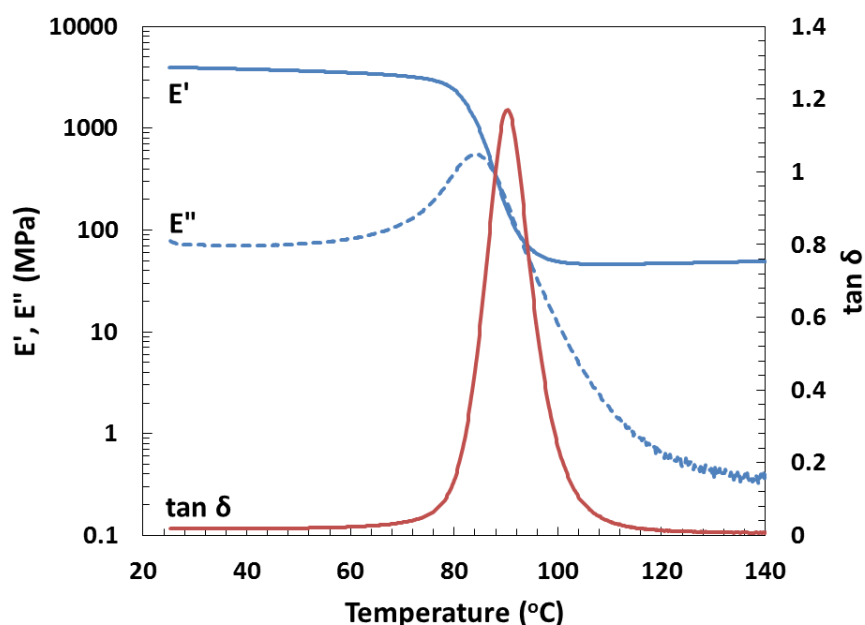
Figure 16. Dynamic moduli as a function of temperature for EPON828/D230/20vol% alumina

2.3.2 Shear Modulus

The shear modulus was measured on the same sample as described for the dynamic modulus tests (Figure 17). The temperature was increased from 30 °C to 150 °C at a rate of 1 °C/min while oscillating at 1Hz and strain amplitude of 1.0% for these tests. The resulting T_g (tan δ peak) is 97 °C.

27
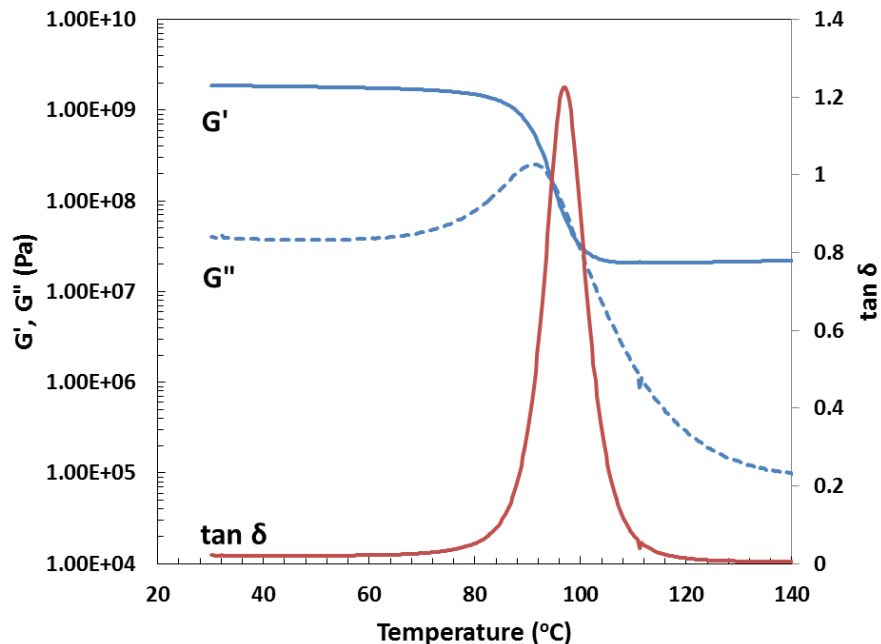
Figure 17. Shear moduli as a function of temperature for EPON828/D230/20vol% alumina

2.3.3 Master Curve

Data for the construction of a master curve were measured in the same manner as described in Section 2.2.3 on a rectangular sample having dimensions 39.10 mm X 9.34 mm X 1.59 mm. The measurements were done in the same order, beginning at the highest temperature and working towards the lower temperatures. Using a reference temperature of 90 °C, the curves were shifted along the frequency axis to obtain the master curve (Figure 18). Note that the shifts were bases solely on the tan δ curves for these plots.
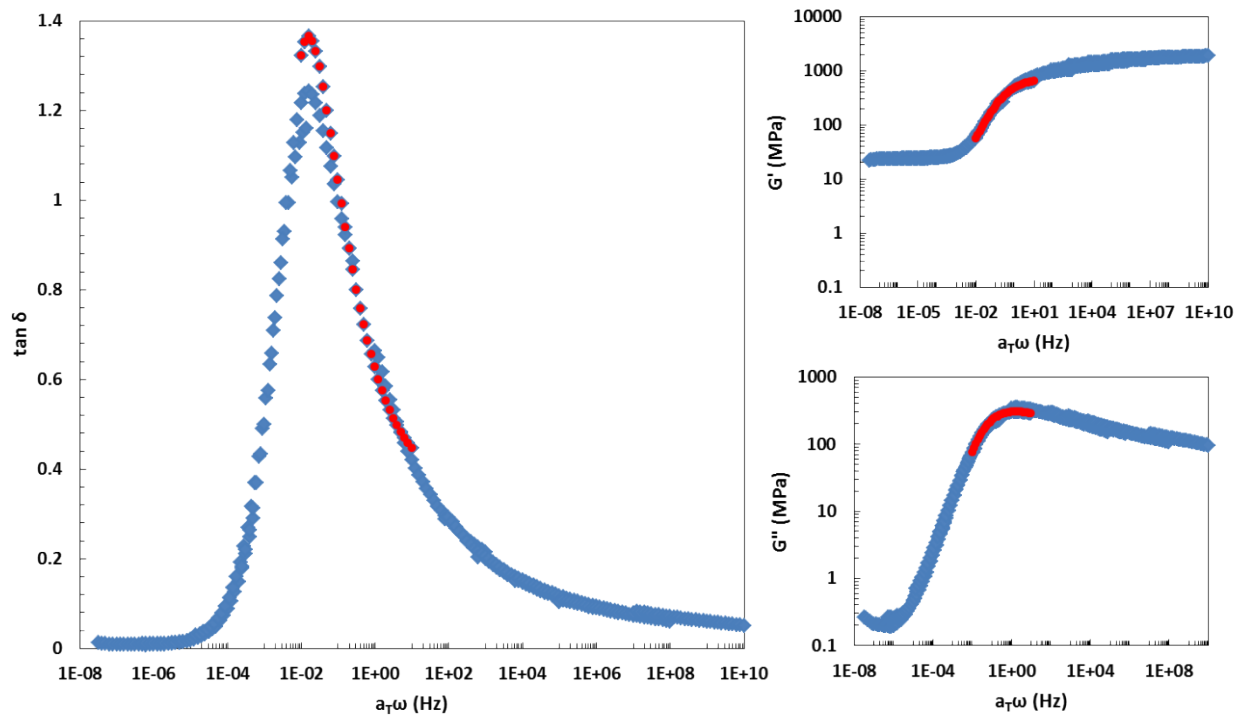
Figure 18. Time-temperature superposition results for EPON828/D230/20vol% alumina with T_{ref} = 90 °C (red points indicated data at T_{ref})

Once the data were shifted, the shift factors were plotted against the associated temperature on a semi-log plot and fit with the WLF equation (Equation 1) giving a good fit for $T > T_g$, as expected (Figure 19). The WLF coefficients obtained from the fit shown below are as follows: C_1 = 11.5 and C_2 = 32.7.
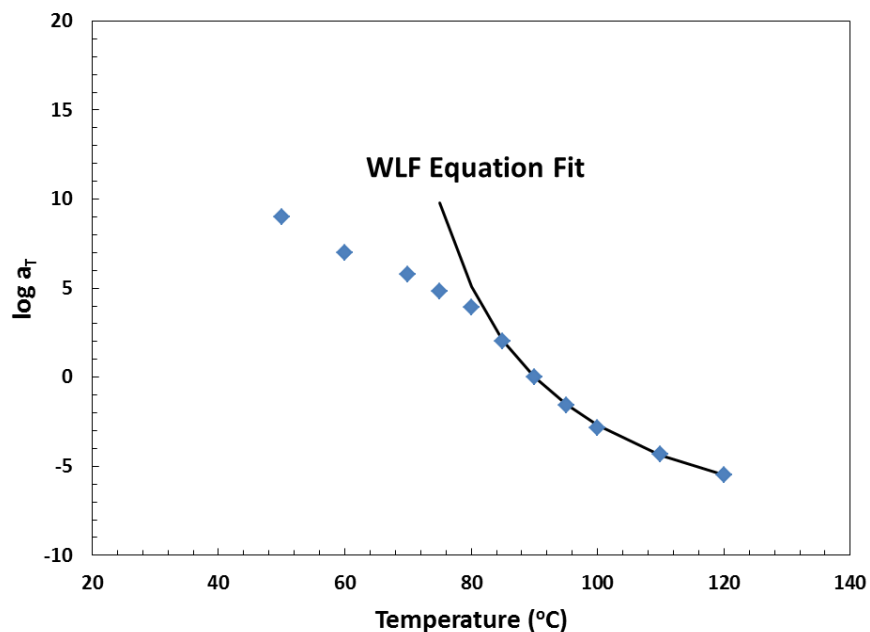
Figure 19. WLF fit to the TTS shift factors for EPON828/D230/20vol% alumina

2.3.4 Thermal Expansion

The thermal expansion behavior was measured on a small rectangular sample having dimensions 9.08 mm X 5.86 mm X 4.72 mm over the temperature range 0 °C to 150 °C while heating at 2 °C/min (Figure 20). Good agreement between heating and cooling curves indicated negligible thermal lag. The rubbery and glassy (room temperature) CTE's are approximately 150 and 35-45 ppm/°C, respectively.
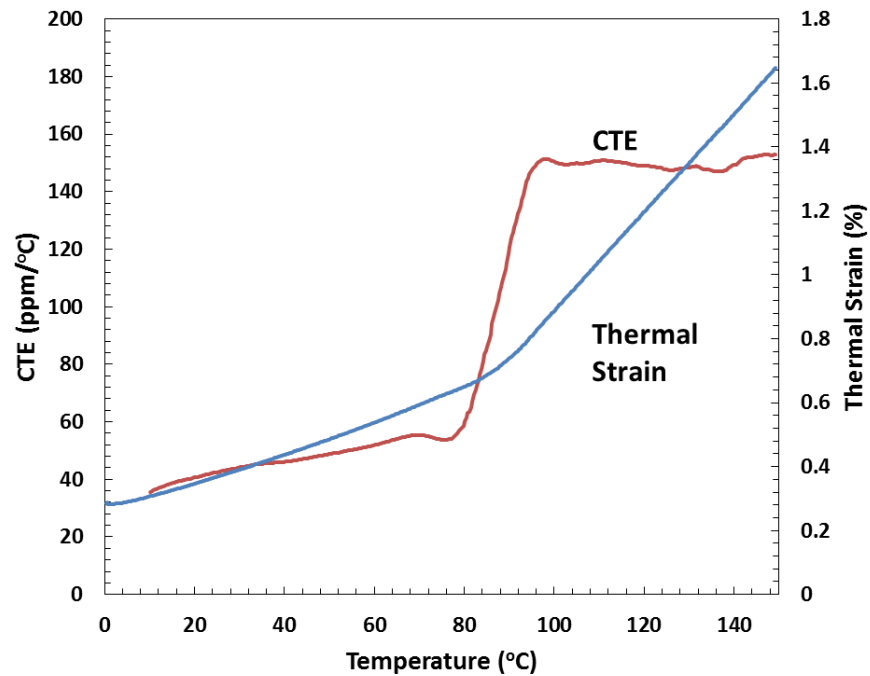
Figure 20. Thermal strain and CTE for EPON828/D230/20vol% alumina

2.3.5 Compression

Compression testing was carried out on cylindrical samples 18 mm tall and having diameter of 8.5 mm. The testing was done as described in Section 2.2.5 at temperatures of -55, -25, 22, and 50 °C (Figure 21).
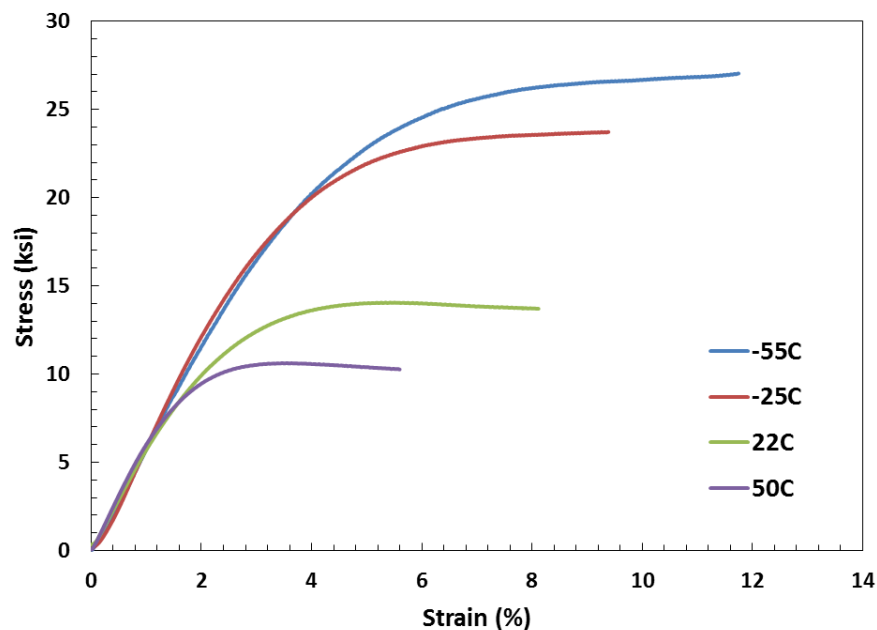
Figure 21. Compressive stress versus strain at various temperatures for EPON828/D230/20vol% alumina

The compressive moduli for EPON828/D230/20vol% alumina derived from the data in Figure 21 are given in Table 3. The lower compressive modulus as compared with EPON828/D230/30vol% alumina is due to the lower amount of filler in the system. There also appears to be a higher dependence of the compressive modulus on temperature at elevated temperatures. This is likely due to the fact that increased filler fraction tends to "mask" the glass transition behavior. Thus, the small filler fraction here simply allows the observance of the onset of the glass transition for temperatures at and above 50 °C.

Table 3. Compressive modulus at various temperatures for EPON828/D230/20vol% alumina

Temperature (°C)	Compressive Modulus* (ksi)	Standard Deviation
-55	501	16
-25	492	8
22	402	16
50	321	36

*average of 4 independent measurements

3. VISCOELASTIC MODELING

To maximize their utility, the above described data for the EPON828/D230/30vol% alumina system were used to parameterize a viscoelastic model to enable predictions of deformation and stress behavior under various environments and geometries. A brief description of the models, the fitting process, and the resulting fits are presented here.

3.1 Potential Energy Clock (PEC) Model

A physically based polymer model must meet certain well-defined criteria drawn from experimental observations. The intrinsic time dependence observed in viscoelastic materials arises from an underlying relaxation mechanism that has been shown to conform to the time-temperature hypothesis of Leaderman.[3] Dissipation, history dependence with fading memory, glass transition, a sensitivity to temperature and a "yield-like" behavior producing highly nonlinear relaxations under excessive stress or strain all strongly favor a nonlinear viscoelastic modeling approach over elasticity or plasticity. The thermorheologically simple behavior[3] is captured readily with a material clock described by the WLF equation[5] in the small strain regime for the equilibrated material above glass transition. However, a nonlinear, thermodynamically consistent formalism is needed to predict properly the acceleration in relaxation rates under finite strains.

To meet these requirements, Caruthers et al.[6] developed a nonlinear viscoelastic formalism whereby the Helmholtz free energy was represented by a second order Frechet series expansion in the temperature and strain histories for a material undergoing finite deformations with fading memory employing a material clock. The proposed Helmholtz free energy served as a potential function from which the stress constitutive equation was derived along with other thermodynamic quantities of interest (e.g., entropy, internal energy). The success of the constitutive framework was secured by two important findings. The first was the identification of the Hencky strain as the appropriate strain measure for the second order expansion. This requirement arose from the need for the first invariant of the strain tensor to be a function of volume only to achieve the incompressibility limit as the material transitioned from the glass into the rubber. The second critical aspect of the model was determining the driving force for the material clock. That was found to be the potential part of the internal energy.

The PEC model was shown to predict a broad range of relaxation phenomena for both thermosets and thermoplastics including temperature and time dependence of stress-strain through "yield", volume and enthalpy relaxation and stress relaxation during multi-step loading histories.[7] Moreover, this was accomplished using a single set of PEC material parameters for each material. There are, however, intrinsic difficulties associated with the use of the PEC model. First, being formulated in terms of the Hencky stress-strain relations, the finite element implementation of the model requires a fourth order tensor transformation to map the logarithmic stress-strain equations into the Cauchy space. This is computationally taxing. Second, there are single and double hereditary integrals requiring four independent relaxation functions stemming from the entropy definition and the volume, shear, and temperature terms in the definition of stress. Although the model is populated exclusively from linear viscoelastic properties using no phenomenological tuning parameters, these viscoelastic functions, properties and all the

associated temperature/volume dependencies must be measured accurately and consistently. That requires an extensive experimental characterization that is time consuming and prohibitively expensive for most engineering applications.

3.2 Simplified Potential Energy Clock (SPEC) Model

To ease the experimental and computational burdens imposed by the PEC formalism, a simplified potential energy clock (SPEC) model[8] was developed. This was accomplished by a combination of steps intended to reduce the complexity of the numerical computations, avoid some of the higher order temperature and volume dependencies and make the material clock more phenomenological by introducing "fitting" parameters. To bypass the calculations of a logarithmic strain and the fourth order tensor transformation needed to compute the Cauchy stress, the Hencky strain rate was approximated by the unrotated rate of deformation tensor, d. Although the integral of the rate of deformation tensor does not yield a true strain measure, it does provide a very close approximation to the Hencky strain for strain levels that would be reasonable for a glassy polymer. The resulting SPEC approximation for the Cauchy stress, σ, is

$$
\begin{aligned}
\underline{\underline{\sigma}}(t) = {} & \frac{\rho}{\rho_{ref}}\left[\Delta K(T)\int_0^t ds\, f_v\!\left(t^* - s^*\right)\frac{dI_1}{ds} - \Delta A(T)\int_0^t ds\, f_v\!\left(t^* - s^*\right)\frac{dT}{ds}\right]\underline{\underline{I}} \\
& + \frac{2\rho\Delta G(T)}{\rho_{ref}}\int_0^t ds\, f_s\!\left(t^* - s^*\right)\!\left[\underline{R}(t)\cdot \underline{\underline{d}}_{dev}(s)\cdot \underline{R}^{-1}(t)\right] \\
& + \frac{\rho}{\rho_{ref}}\left[K_\infty(T)I_1(t) - A_\infty(T)\{T(t) - T(0)\}\right]\underline{\underline{I}} \\
& + \frac{2\rho G_\infty(T)}{\rho_{ref}}\left[\underline{R}(t)\cdot \underline{\underline{\varepsilon}}_{dev}(t)\cdot \underline{R}^{-1}(t)\right]
\end{aligned}
\tag{2}
$$

In this equation, ρ and ρ_{ref} are the densities at the current state and reference state, f_v and f_s are normalized volumetric and shear relaxation spectra which decay from 1 to 0, R is the rotation tensor, I is the identity tensor, ε is the strain computed from the integral of the rate of deformation tensor, I_1 is the trace of the strain tensor, T is temperature, and the "dev" subscript denotes the deviatoric part of the designated tensor. The prefactors in the above equations are parameters that must be determined for each specific material. In general, they are related but not identically equal to the more commonly recognized bulk and shear moduli, K and G, and thermal expansion coefficient, α, as follows. A temperature dependence in these prefactors, denoted by (T) in the equations below, is allowed.

$$\Delta K(T) = K_g(T) - K_\infty(T) \tag{3}$$

$$\Delta G(T) = G_g(T) - G_\infty(T) \tag{4}$$

$$\Delta A(T) = \left[K_g\alpha_g - K_\infty\alpha_\infty\right](T) \tag{5}$$

The subscripts "∞" and "g" are applied to designate the "equilibrium" and "glassy" values of a designated parameter. The material clock is defined by a shift factor, "a", based on a re-definition of the potential energy found in the PEC model.

$$t^* = \int\limits_0^t \frac{dw}{a(w)} \tag{6}$$

$$\log\left[a(t)\right] = -\frac{C_1 N(t)}{C_2 + N(t)} \tag{7}$$

$$N(t) = \left\{\left[T(t) - T_{ref}\right] - \int\limits_0^t ds\, f_v\left(t^* - s^*\right)\frac{dT}{ds}(s)\right\}$$
$$+ C_3\left\{I_1(t) - \int\limits_0^t ds\, f_v\left(t^* - s^*\right)\frac{dI_1}{ds}(s)\right\} \tag{8}$$
$$+ C_4\left\{\int\limits_0^t ds\, f_s\left(t^* - s^*\right)\underline{\underline{d}}_{dev}(s)\right\} : \left\{\int\limits_0^t ds\, f_s\left(t^* - s^*\right)\underline{\underline{d}}_{dev}(s)\right\}$$

The coefficients C_1 through C_4 are phenomenological and must be fit to data. For an equilibrated material undergoing free thermal expansion/contraction above the glass transition temperature, the integrals are identically zero and the material clock depends on temperature and volume only.

Although the experimental characterization and model calibration process is easier for the SPEC model than the PEC model, the performance predictions are quite comparable. The SPEC approximations have been shown to be entirely suitable for engineering applications[7] having been applied to unfilled thermosets and thermoplastics as well as epoxies with particulate fillers that were characterized as an isotropic homogeneous continuum.

3.3 Material Characterization and SPEC Model Calibration

Perhaps the most formidable challenge of viscoelastic modeling arises from the time, expense and difficulty in performing the requisite material characterization and model calibration. In general, the SPEC model requires data to define the two relaxation spectra, the decaying prefactors for the hereditary integrals and the corresponding equilibrium parameters. This leads naturally to three classes of experiments involving shear, temperature and volume.

The shear tests are relatively straightforward. The glass transition temperature (T_g) and modulus temperature dependence can be obtained with a Dynamic Mechanical Analyzer (DMA) measuring the storage and loss moduli during torsion at fixed frequency while sweeping the temperature at a constant rate from the glassy to the rubbery states. The shear master curve is built following the conventional approach for thermorheologically simple materials. Here, the DMA test protocol is changed to measure dynamic properties across a range of frequencies during isothermal tests conducted at different temperatures taken around glass transition. At each temperature, the shear storage and loss moduli, G' and G'' respectively, are measured and

tan δ is computed as the ratio of the two values (tan delta = G''/G'). These data then are plotted versus the logarithm of frequency producing a family of curves, one for each test temperature. The master curve is generated from the tan delta plots by first choosing a reference temperature (T_{ref}) curve and horizontally shifting all remaining curves on the log frequency axis to obtain a smooth, continuous, composite representation of the function. By performing the horizontal shifts with the tan δ curves, the modulus temperature dependence cancels out and the need for vertical shifts is removed. Once the horizontal shift factors have been defined from the tan δ curves, the master curves for storage and loss moduli are constructed by applying the same horizontal shifts. In this case, some vertical shifts may be necessary to accommodate small changes in moduli with temperature. Although this produces master curves in the frequency domain, viscoelastic analyses utilize relaxation functions in the time domain. That requires an additional mapping facilitated by an exponential series expansion (Prony series) providing a convenient representation for the shear relaxation spectrum as follows:

$$G(t) = G_\infty + \Delta G \sum_{i=1}^{N} f_i \exp(-t / \tau_i) = G_\infty + \Delta G f_s(t) \tag{9}$$

The values f_i and τ_i are fitting constants. When the exponential series is substituted into the linear viscoelastic shear hereditary integral and the stress is computed for a sinusoidal, constant amplitude shear strain history, $\gamma_o \sin(\omega t)$, expressions are obtained for the storage and loss moduli in terms of the exponential series parameters and the frequency, ω:

$$G'(\omega) - G_\infty = \Delta G \sum_{i=1}^{N} f_i (\omega \tau_i)^2 / \left[1 + (\omega \tau_i)^2 \right] \tag{10}$$

$$G''(\omega) = \Delta G \sum_{i=1}^{N} f_i (\omega \tau_i) / \left[1 + (\omega \tau_i)^2 \right] \tag{11}$$

The latter two equations are suitable for fitting the shear storage and loss master curves in the frequency domain. When the fitting constants are defined, the relaxation spectrum in the time domain is computed directly from Equation 9.

The bulk modulus and its temperature dependence can be measured with a pressure-dilatometer. This often is achieved by applying strain gauges to a protected sample pressurized in a fluid bath. Mapping the bulk relaxation spectrum, f_v, directly by measuring the time dependence of the decaying pressure following step changes in volume at different temperatures is much more cumbersome. Fortunately, there is an alternative resulting from the fact that the SPEC model uses a single relaxation function for both the bulk and temperature hereditary integrals. Thermal strain data collected with a Thermal Mechanical Analyzer (TMA) provide another means of calibrating the model. Since the location and shape of the glass transition are determined by the prescribed temperature history, a properly calibrated constitutive equation must be able to predict the heating and cooling strains from an analysis of the actual test conditions. That suggests the possibility of using an iterative modeling approach to deduce the prefactors and relaxation function required to minimize the error between predictions and data. Starting from an assumed

property set, the SPEC model is used to predict the thermal strain response during a temperature history cycling through glass transition at prescribed rates. The resulting strain-temperature curves are compared to the measured data, and model parameters are adjusted to minimize the error. The slopes of the glassy and rubbery response contribute to the definition of the prefactors in Equations 3 and 5. The parameterization of the relaxation function is facilitated by simplifying the functional form to a stretched exponential. This allows the minimization of error from the relaxation function to be controlled through the specification of only two parameters, λ and β:

$$f_v(t) = \exp\left(-(t/\lambda)^\beta\right)$$
(12)

In general, the stretched exponential still must be converted to a Prony series for ease of constitutive computations. However, by specifying a fixed distribution of relaxation times, the Prony prefactors are solved readily from a linear set of equations. Surprisingly, the iterative process of parameterization works very well and is easily executed with a finite element analysis in a one-element problem.

Through a judicious choice of C_1 and C_2, the material clock equation for the logarithm of the shift factor can be reduced to the familiar WLF form for an equilibrated material. The C_3 parameter defines the pressure dependence of the glass transition temperature while C_4 governs the nonlinear relaxations producing "yield-like" behavior under loading. The C_4 parameter is chosen to reproduce stress-strain data like that obtained from a compression test.

3.4 SPEC Model Calibration for EPON828/D230/30vol% Alumina

Following the procedures detailed above and the data reported in Section 2.3, the SPEC model was calibrated for the EPON828/D230/30vol% alumina material and a summary of the process and resulting fits is presented here. First, the time-temperature superposition data were shifted to produce a master curve in the frequency domain (Figure 22a) in terms of tan δ ($T_{ref} = 90$ °C). The shift factors used to obtain this master curve are shown, along with the WLF equation fit, in Figure 22d ($C_1 = 16$, $C_2 = 57$). Then, the G' and G" curves were shifted using the same shift factors (Figure 22b,c). Slight vertical shifts were also employed to obtain these two curves to compensate for the temperature dependence of the moduli.
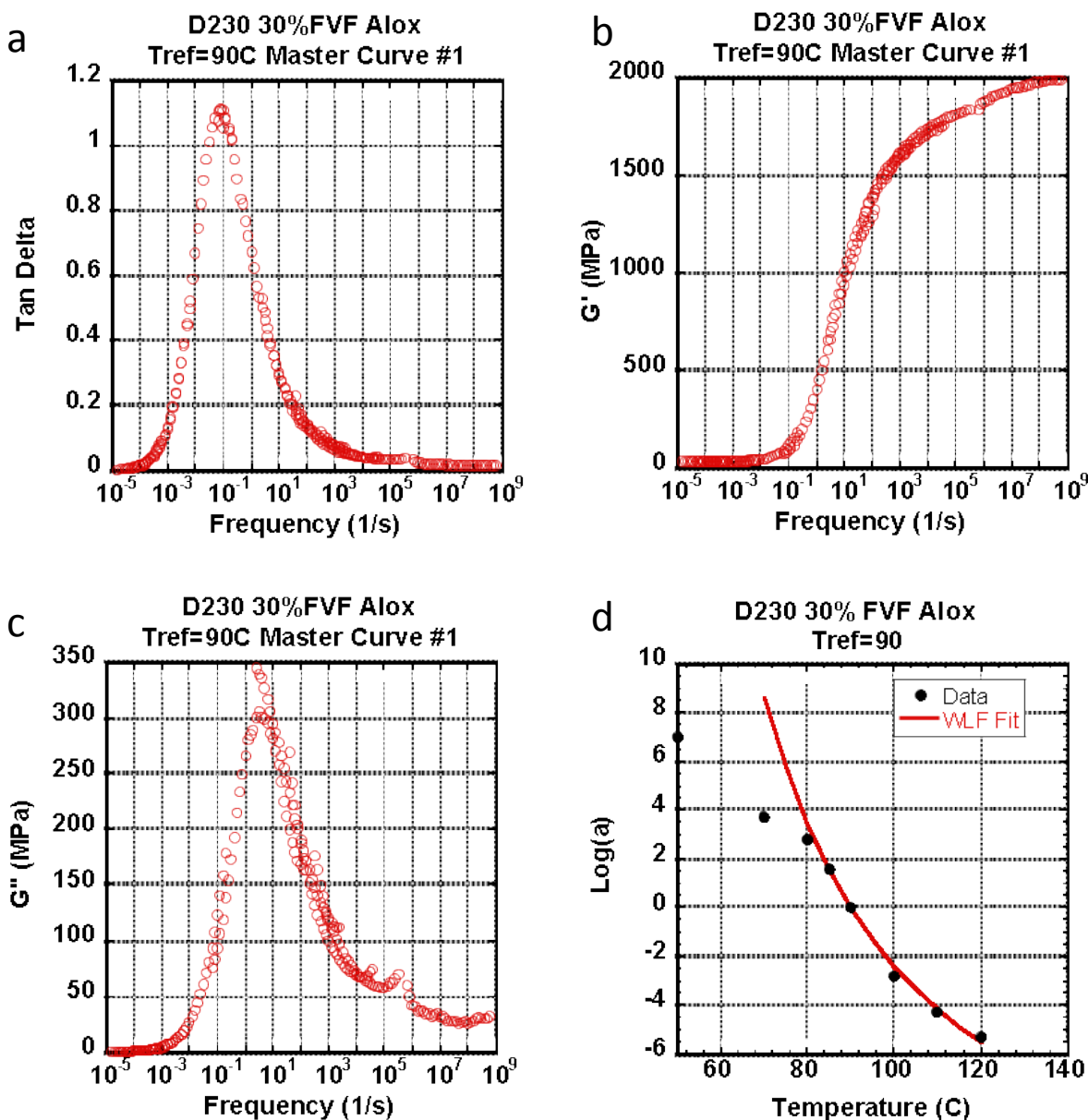
Figure 22. TTS and shift factors, including vertical shifts, for EPON828/D230/30vol% alumina

Next, the temperature dependence of the glassy shear modulus was determined from the slope of the G' versus temperature data shown in (Figure 11). This was done by taking the slope of a line fit to the data at temperatures below 50 °C. The resulting temperature dependence was determined to be about -5 to -6 MPa/°C.

The next step in the SPEC model calibration was to convert the master curve from the frequency domain to the time domain through a Prony series. The G' versus frequency and G" versus frequency curves were concurrently fit with a Prony series to define the fitting parameters in Equations 10 and 11 (Figure 23). The resulting Prony series fit nicely represents the experimental, shifted data for EPON828/D230/30vol% alumina.
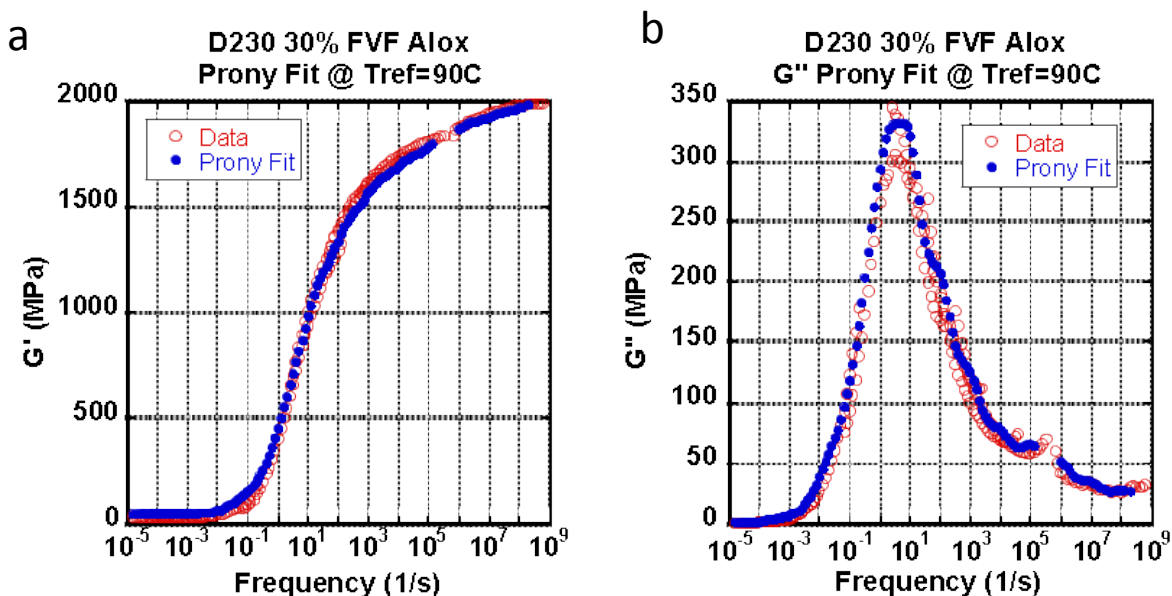
Figure 23. Prony series fits to G' and G" data for EPON828/D230/30vol% alumina

Once the fitting parameters were obtained from the Prony series fit to the G' and G" master curves, the shear relaxation modulus was computed using Equation 9 (Figure 24). Thus, the transformation of the master curve from the frequency domain to the time domain was complete.
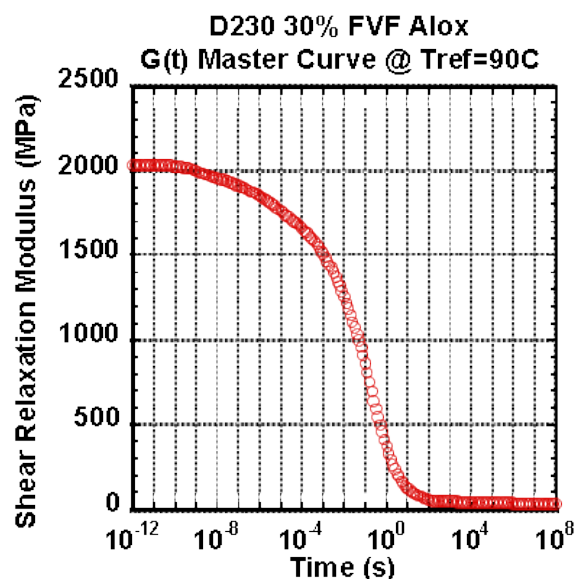
Figure 24. Shear relaxation modulus in the time domain from master curve for EPON828/D230/30vol% alumina

Next, an iterative approach was used, based on the thermal strain data (Figure 14) to define the parameters in Equation 12. A property set was assumed and the thermal strain calculated based on the assumed properties. The calculation was then compared to experimental data and the properties and parameters adjusted to minimize the error. Figure 25 shows very good agreement

and fit between the calculated and experimental linear thermal strain and inflection at the glass transition.
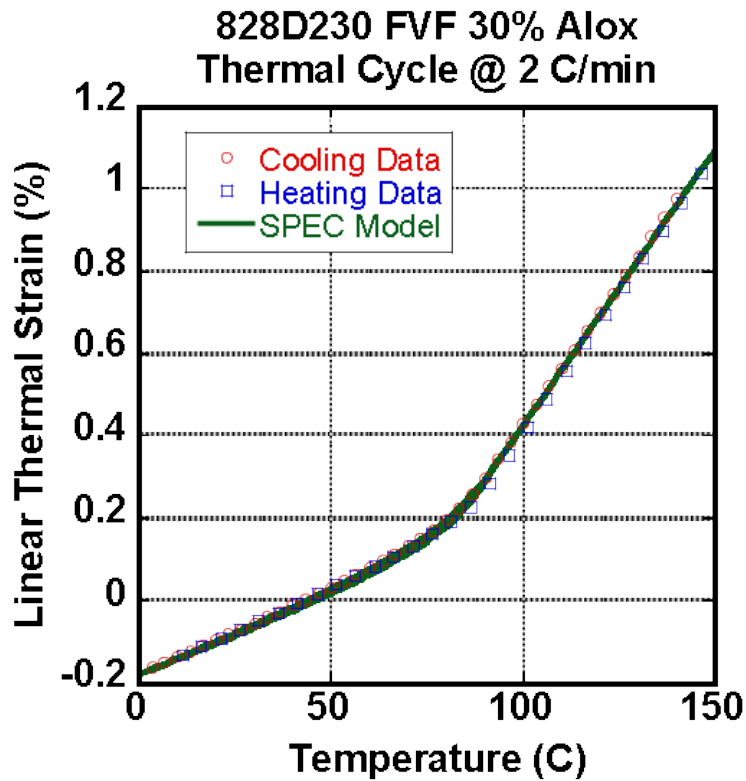
Figure 25. SPEC model fit to thermal strain data for EPON 828/D230/30vol% alumina

Finally, the stress versus strain response and yield behavior were used to define the C_4 clock parameter in the SPEC model. Figure 26 shows good agreement between experimental and predicted compressive stress/strain response of EPON828/D230/30vol% alumina at a wide range of temperatures below T_g.
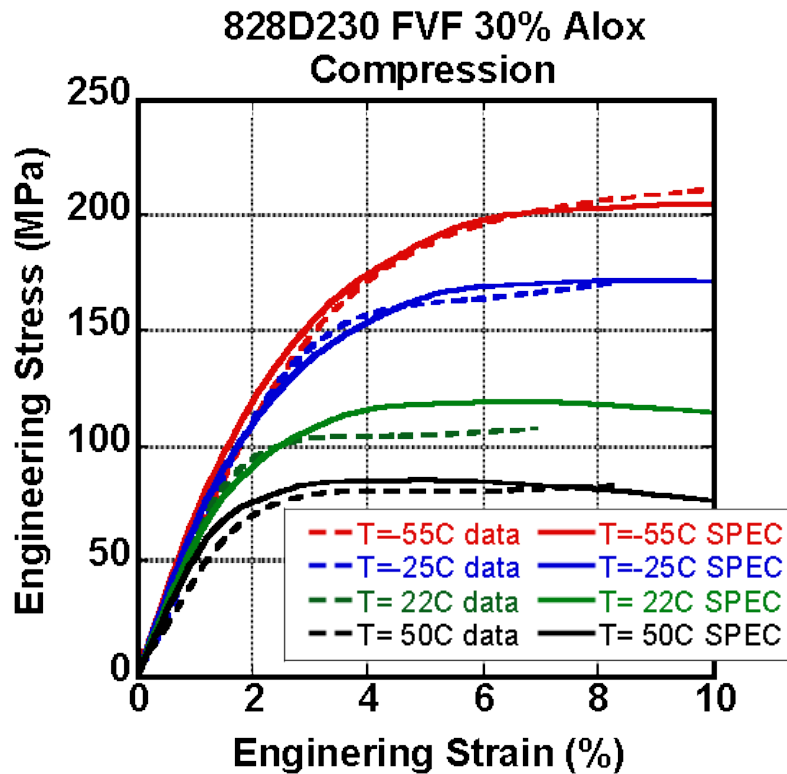
Figure 26. SPEC model predictions of compressive stress-strain at various temperatures for EPON828/D230/30vol% alumina

Using the process discussed above, the SPEC model was completely calibrated to the EPON828/D230/30vol% alumina material with very good results. Using the parameters established here, the SPEC model can now be used to give an accurate representation of this material at various temperatures, conditions, and geometries. The parameters defining the model, derived from experimental data, are summarized in Appendix A.

4. RELATIVE CURE AND THERMAL STRESS COMPARISON

Another important consideration when using thermosetting materials, especially in highly confined environments such as beneath a PBGA, is the shrinkage experienced by the material both during cure and cooling from the cure temperature to room temperature. Both of these material contractions result in an accumulation of stress in the material. However, the separation of the two (i.e. cure stress vs. thermal stress) is not always straightforward. During the cure reaction the material contracts as bonds or crosslinks are chemically formed which constrain the polymer chains. In essence, there is a loss of free volume as the crosslinking reaction progresses. Concurrent with this, the modulus of the material is increasing. Since these two events happen simultaneously, it is difficult to quantify cure stress as the product of an evolving modulus and a strain (from shrinkage). Further, to get a good estimate of the cure shrinkage and stress apart from the thermal shrinkage, the measurement must be done at temperature without cooling the material for analysis. Again, this adds complexity to the problem.

As part of this work, a method was developed which allows the relative comparison of the cure and thermal shrinkage during the cure of a material and its subsequent cooling to room temperature. Further, using this method for multiple materials allows a relative qualitative comparison of the materials. Quantitative estimations of the resulting stresses were not possible given the time and resource constraints of this project.

In order to qualitatively asses the shrinkage during cure and cooling, a bi-material beam test was utilized. In this test a thin layer of the thermoset material was cast onto a thin metal substrate using a tape-caster to ensure a uniform thickness. The coated beam was then put into a preheated oven and fixed on one end (Figure 27a). As the thermoset cures and shrinks, it causes the unconstrained end of the beam to deflect upwards (Figure 27b). The deflection is monitored optically over time. At the end of the cure, the sample is removed from the oven and allowed to cool to room temperature. As the bi-material beam cools, the beam deflects more due to the difference in coefficients of thermal expansion between the aluminum and the thermoset (with the thermoset generally having the higher CTE, Figure 27c). The final deflection is a result of both the thermal contraction and the cure shrinkage experienced in the thermoset material. Generally, a higher amount of deflection is related to a higher degree of shrinkage. Again, the actual stress generated from these two processes was not calculated here and further study to obtain quantitative results is warranted. The testing done here simply provided a qualitative comparison between two candidate materials.
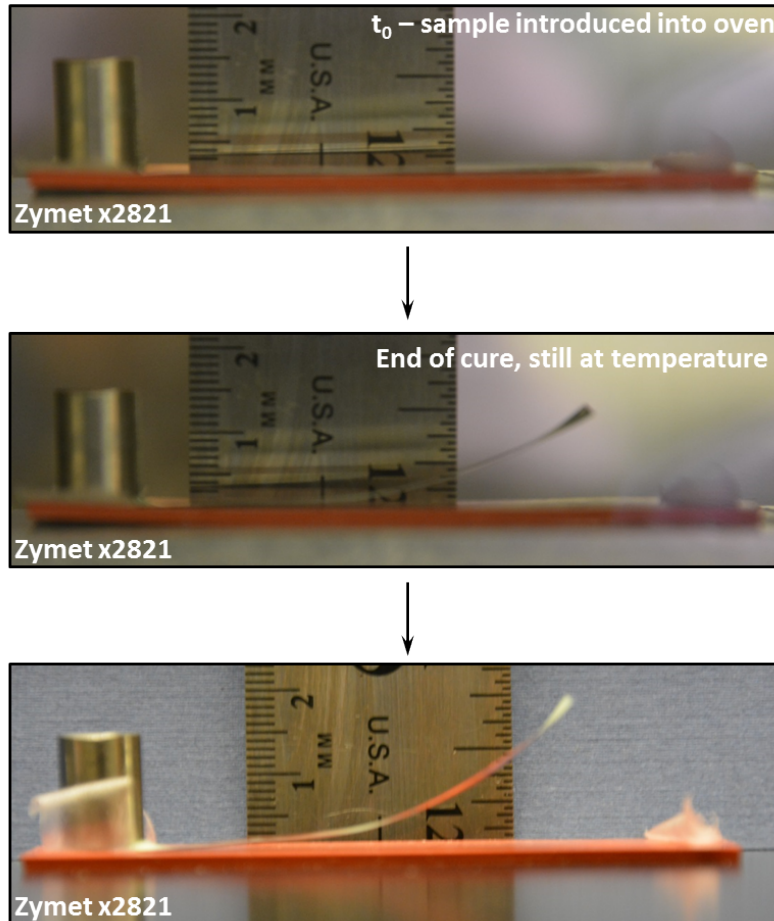
Figure 27. Representative example of a bi-material strip test

The bi-material strip test was first done with the Zymet X2821 material. Zymet was cast onto an aluminum strip having thickness 0.005" and measuring 7 mm wide and approximately 50 mm long. The composite strip was then placed on a silicone pad material to simulate the processing done during PBGA underfill operations. The pad and bi-material strip were then place into a preheated 120 °C oven for a total of 10 minutes to cure the Zymet X2821. Following the 10 minute cure, the bi-material strip and silicone pad were removed from the oven to the lab bench where they were allowed to cool to room temperature. Throughout the process, photos were taken of the strip with a ruler in the background to monitor the beam deflection. A representative set of data showing the magnitude of the deflection as a function of time is shown in Figure 28.
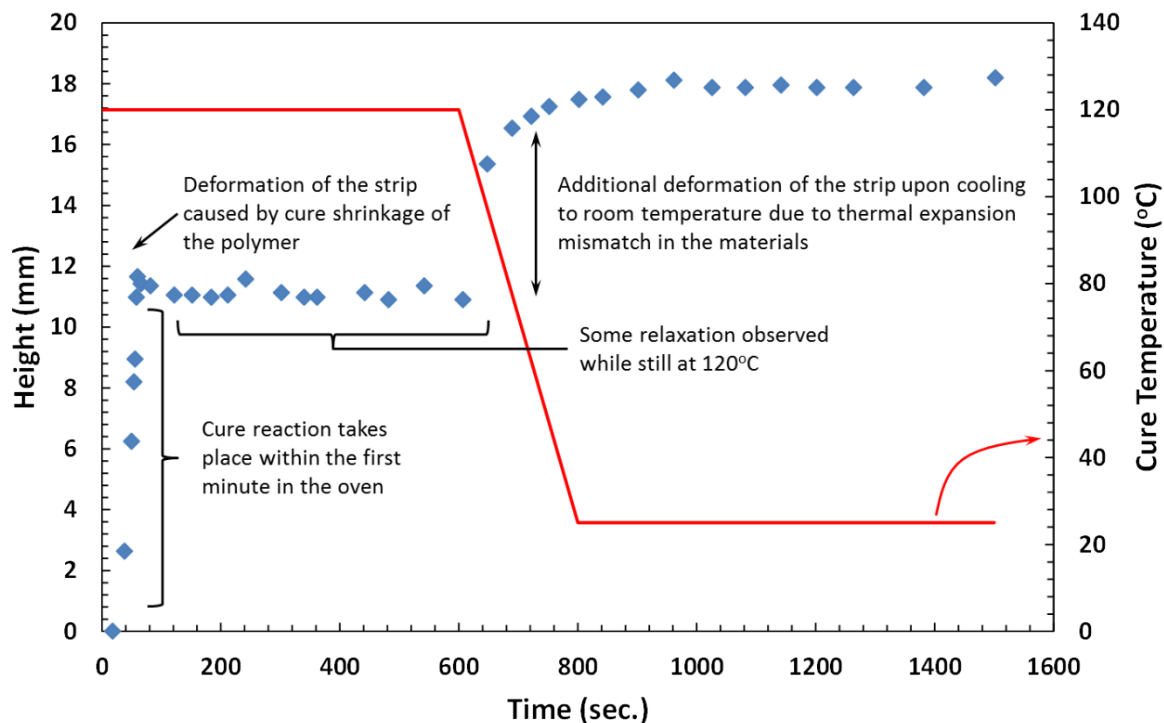
Figure 28. Beam deflection as a function of time for a sample of Zymet X2821 on an aluminum beam during 120 °C cure and cooling to room temperature

The cure reaction of Zymet X2821 under these conditions is essentially complete within the first minute in the oven. During this time the unconstrained end of the bi-material strip deflected approximately 12 mm. There was some relaxation of the deflection over the ensuing 8-9 minutes. The sample was then removed from the oven and additional deflection was observed as it cooled to room temperature. The additional deflection due to thermal shrinkage amounted to approximately 6 mm for a total deflection of about 18 mm. From this and subsequent repeats of this test, it was observed that approximately 50-60% of the total deformation occurred during the cure of the Zymet X2821 with 40-50% of the deformation occurring during the cool down from 120 °C to room temperature.

Next, this same procedure was repeated using EPON828/D230/30vol% alumina with its associated cure schedule (Figure 29). Again, there was measureable deflection in the unconstrained end of the beam during cure and significant deflection during the cool down from 80 °C to room temperature. However, the deformation did not appear until very late in the cure for the alumina filled EPON828/D230. Measureable deflection was not observed until about half way through the second stage of the cure schedule. Note that the two stage cure may help to alleviate some of the deflection as the ramp from 50 °C to 80 °C may help to balance the shrinkage due to cure with the thermal expansion due to the increasing temperature. At the end of the cure schedule the total deflection of the beam was approximately 2 mm. Upon cooling to room temperature the total deflection was approximately 10 mm. Thus, only about 20% of the total deflection can be attributed to the cure shrinkage while 80% is attributed to thermal contraction.
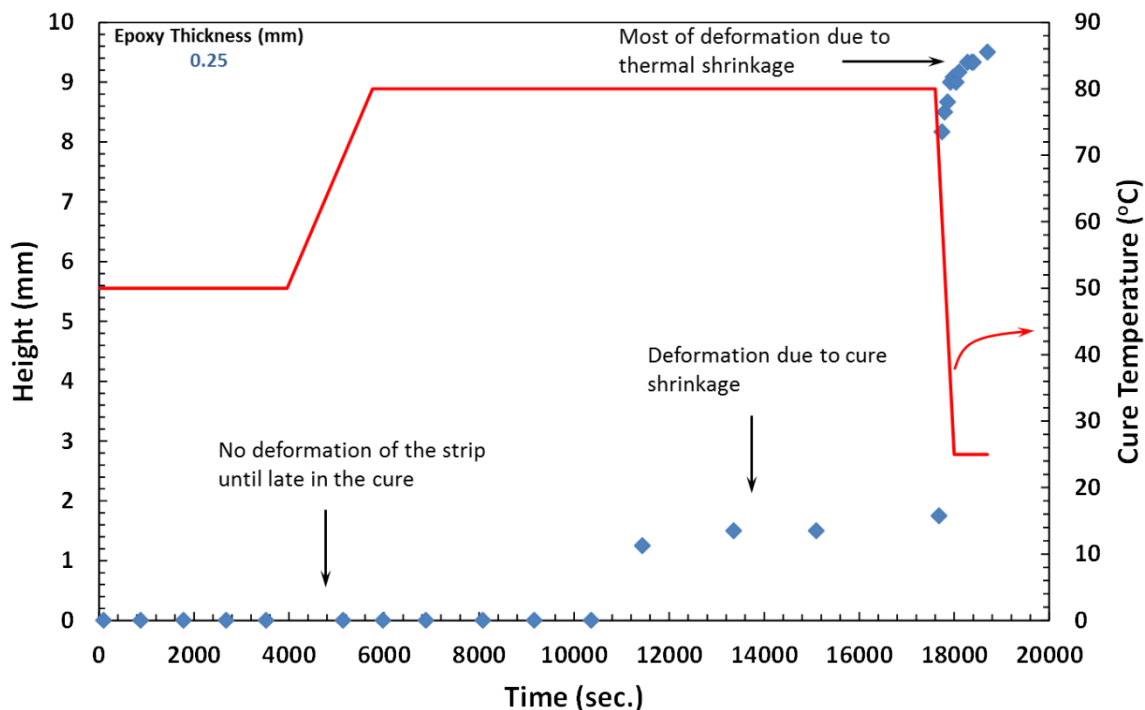
Figure 29. Beam deflection for EPON828/D230/30vol% alumina as a function of time during cure and cooling to room temperature

Lastly, a comparison was made between the deformation associated with the Zymet X2821 and the EPON828/D230/30vo% alumina (Figure 30). To enable a comparison, the measurement time was normalized by the total time of the experiment (including cure and cool down). These data show a stark comparison in the deformation behavior of the bi-material strips composed with the two thermosets studied here. The EPON828/D230/30vol% alumina shows a much smaller amount of both cure and total deformation when compared to the Zymet X2821. In fact, the Zymet X2821 produced almost as much deformation during cure as the EPON828/D230/30vol% alumina produced in total. Further, the total deformation exhibited by the EPON828/D230/30vol% is roughly half of the total deformation exhibited by the Zymet X2821. One possible contributor to the differences in deformation due to cure alone is that for the Zymet X2821 the material vitrifies during cure while the bulk of the cure in EPON828/D230/30vol% alumina occurs in the rubbery regime (i.e., $T < T_g$). While in the rubbery state, the polymer chains have much more mobility and are better able to relax when compared to the glassy regime.
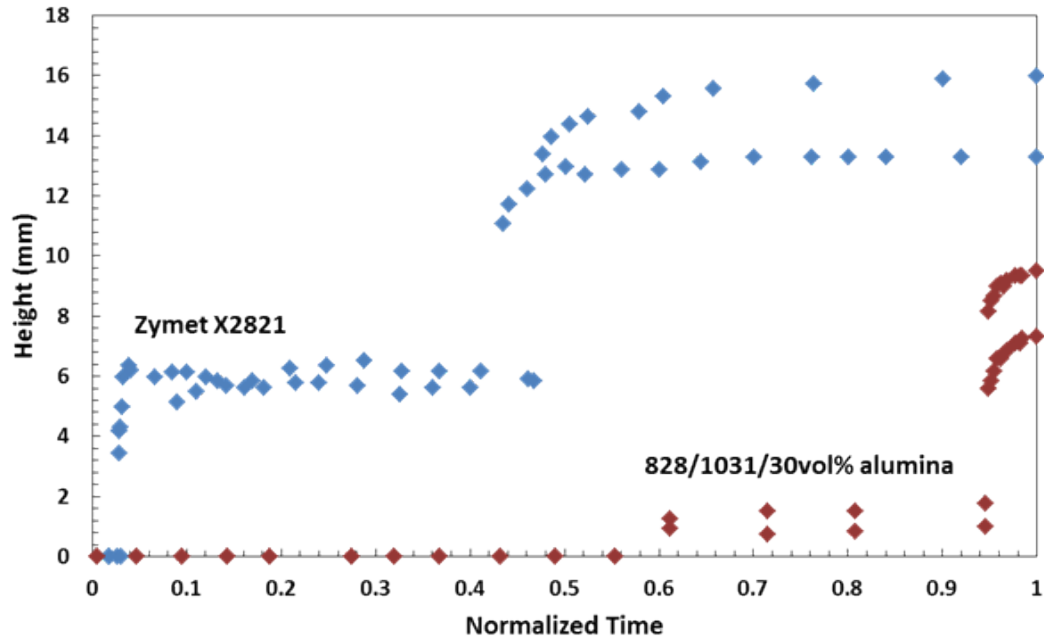
Figure 30. Beam deflection comparison for Zymet X2821 and EPON828/1031/30vol% alumina during cure and cooling to room temperature

Because time and resources were limited in the present study, these tests were not done with the EPON828/D230/20vol% alumina system. However, it is expected that the results would lie somewhere between the 30vol% filled system and the Zymet X2821. The main driver for this difference is expected to be the relatively higher CTE due to the lower filler fraction.

Also due to the constraints faced during this work, efforts were not made to quantify the final stress state of the thermoset material. This remains an important avenue of future work. One potential method to determine the actual stress may be to slowly heat the bi-material strip to the point where all deformation is removed. This would essentially be a measure of the stress-free temperature of the material as-cured. Then a measurement of the deflection when that sample was cooled to room temperature could be used along with some beam theory to calculate an associated stress. Further work could then be done to determine methods to reduce the total stress, if desired.

5. ADHESION TESTING

For a final comparison between the underfill materials studied here, adhesion testing was performed using a napkin ring geometry (Figure 27). For these tests, a sample of underfill was cured in an annular region between two stainless steel plugs with a bondline thickness of approximately 0.020". The test fixtures we then mounted in a torsional Instron and twisted to failure at a rate of 0.1 degrees/sec while measuring the force and angular displacement. The adhesive strength is then taken as the peak torque sustained before break.
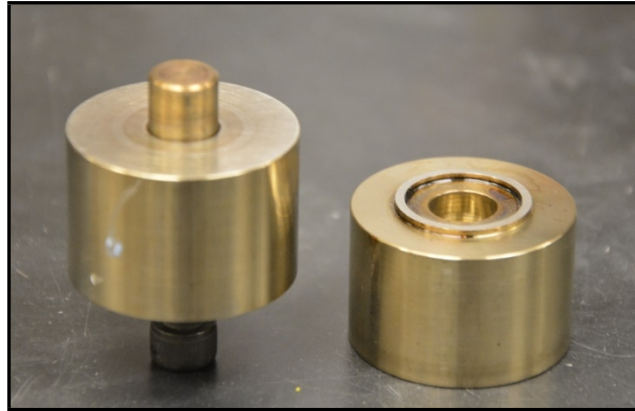
Figure 31. Napkin ring fixture for testing adhesive strength

For each material tested, there was no statistically significant difference in the torque to failure at room temperature indicating a comparable adhesive strength amongst the materials (Figure 28). The Zymet X2821 material was also tested at 70 ^{o}C. At this higher temperature, the torque to failure was similar to that of the 20 vol% alumina at room temperature. These results are significant because at 70 ^{o}C the Zymet X2821 material is a similar (not equal) distance from T_g as the EPON828/D230/20 vol% alumina material is when it is at room temperature. The adhesion testing results show that, at similar distances from their respective T_g, the materials tested here behave in a similar way and show similar adhesive properties.
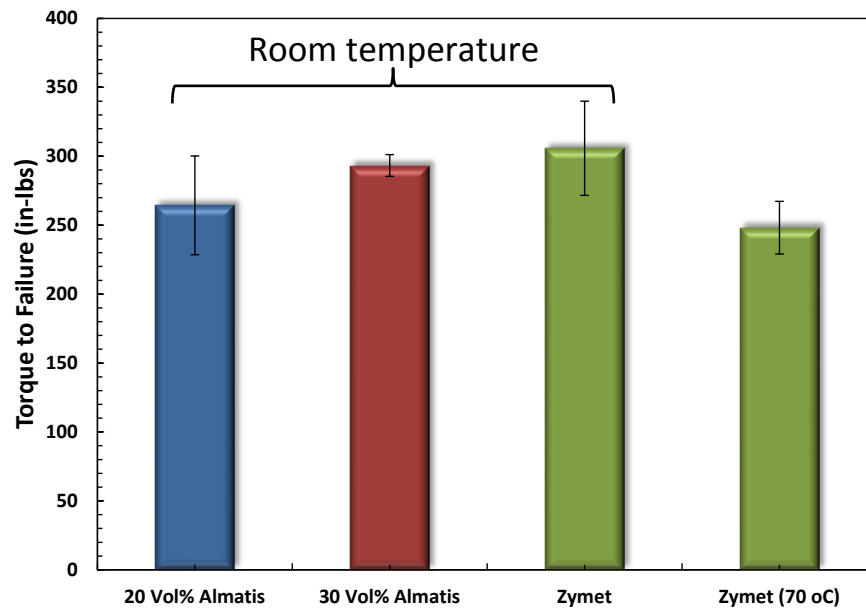
Figure 32. Torque to failure for underfill materials in a napkin ring geometry at room temperature and 70 °C (Zymet X2821 only)

6. FUTURE WORK

The results presented here include a full viscoelastic characterization and model parameterization for the EPON828/D230/30vol% alumina material. These experimental data and modeling fits will prove invaluable to making predictions of underfill behavior in various environments and geometries. Unfortunately, the time and resources were not available to provide the same model parameterization and fits for the 20 vol% alumina material and the Zymet X2821. While preliminary attempts were made with the 20 vol% alumina material, difficulties were encountered during the modeling fits to the experimental data in the vicinity of T_g. We suggest some additional attention be given to the measurements in this region. Perhaps a set of creep and/or stress relaxation tests in this temperature range could be endeavored to provide some supporting information in terms of the stress relaxation modulus to guide the modeling. As a promising underfill material, the modeling aspects for this material should be made a priority.

Further, the snap-cure chemistry exhibited by the Zymet X2821 material is a very new chemistry to Sandia. As industry moves more and more towards these fast curing systems for electronic products/processes, it would be wise to gain some additional experience in the area of these types of underfills. Again, attention should be given to understanding the cure kinetics and how best to control them and how the associated exothermic reactions affect the temperature of surrounding components. Learning how best to model and represent this material in simulations is also important and warrants further exploration. Understanding how the very fast cure reaction affects the cure stress, residual stress, and cure shrinkage is also imperative to understanding this material in underfill applications.

In this report we describe a novel method of comparing the relative deformations due to cure and thermal shrinkage (bi-material strip) for two materials. The comparison here should be extended to the third material – EPON828/D230/20vol% alumina for completeness. Further, more experimental work coupled with modeling is warranted in order to translate the results obtained from the bi-material strip into quantitative results rather than simply comparative results. Being able to quantify the stresses generated during cure and subsequent thermal changes would be an invaluable addition to the material data presented here.

7. CONCLUSIONS

The thermal-mechanical properties of three candidate underfill materials have been measured and reported here (Zymet X2821, EPON828/D230/30vol% alumina, EPON828/D230/20vol% alumina). The first material is a commercial material characterized by a snap-cure chemistry (Zymet X2821) and was found to exhibit interesting behaviors such as a relatively smaller difference in glassy and rubbery moduli than is found in other thermosets. Further, the very fast reaction has been shown to be accompanied by a significant temperature increase in certain geometries. The other materials were developed at Sandia for underfill applications and have also been characterized in terms of their thermal-mechanical behavior.

The 30vol% alumina filled EPON828/D230 material has been fully characterized and fit with the simplified potential energy clock model. The modeling fits are remarkably good and provide the basis for making viscoelastic predictions for this material under various environments and geometries. There was insufficient time and funding to provide similar fits for the other two materials studied here. This certainly warrants some additional attention.

Lastly, a novel method for comparing the relative deformation caused by cure and thermal shrinkage for various materials using a bi-material strip was also presented. Using this method it was shown that the Zymet X2821 material results in a total deformation that was roughly double that of the EPON828/D230/30vol% alumina material. Further, the total deformation from the EPON material was roughly equivalent to that observed from cure alone for the Zymet X2821. This allowed a comparison of the materials and a qualitative comparison for the residual stress that would accompany these materials in an underfill environment.

4. REFERENCES

1. K. Gilleo and D. Blumel, New Generation Underfills Power the 2nd Flip Chip Revolution, in *Pan Pacific Microelectronics Synmposium*, held in Mauna Lani, HI, February 10-13, 1998. Surface Mount Technology Association, Edina, MN, 1998.
2. M. C. Celina, N. H. Giron, T. M. Alam, C. D. Mowry, and A. S. Pimentel, *Analysis and Characterization of Zymet Underfill Epoxy Material*, SAND2015-4686, Sandia National Laboratories, Albuquerque, NM, May 2015.
3. H. Leaderman, *Elastic and Creep Properties of Filamentous Materials*, The Textile Foundation, Madison, WI, 1943.
4. F. Schwarzl and A. J. Staverman, Time-Temperature Dependence of Linear Viscoelastic Behavior, *J Appl Mech*, vol. 23(8), pp. 838-843, 1952.
5. M. L. Williams, R. F. Landel, and J. D. Ferry, The Temperature Dependence of Relaxation Mechanisms in Amorphous Polymers and Other Glass-forming Liquids, *J Am Chem Soc*, vol. 77(14), pp. 3701-3707, 1955.
6. J. M. Caruthers, D. B. Adolf, R. S. Chambers, and P. A. Shrikhande, A Thermodynamically Consistent, Nonlinear Viscoelastic Approach for Modeling Glassy Polymers, *Polymer*, vol. 45(13), pp. 4577-4597, 2004.
7. D. B. Adolf, R. S. Chambers, and J. M. Caruthers, Extensive Validation of a Thermodynamically Consistent, Nonlinear Viscoelastic Model for Glassy Polymers, *Polymer*, vol. 45(13), pp. 4599-4621, 2004.
8. D. B. Adolf, R. S. Chambers, and M. A. Neidigk, A Simplified Potential Energy Clock Model for Glassy Polymers, *Polymer*, vol. 50(17), pp. 4257-4269, 2009.

APPENDIX A: SPEC MODEL DEFINITION PARAMETERS

$K_g = 7\,GPa$

$\dfrac{dK_g}{dT} = -17\,MPa/C$

$K_\infty = 4\,GPa$

$\dfrac{dK_\infty}{dT} = -17\,MPa/C$

$G_g = 2.032\,GPa$

$\dfrac{dG_g}{dT} = -5\,MPa/C$

$G_\infty = 29.1\,GPa$

$\dfrac{dG_\infty}{dT} = 0$

$\alpha_g = 105\,ppm/C$

$\dfrac{d\alpha_g}{dT} = 0$

$\alpha_\infty = 400\,ppm/C$

$\dfrac{d\alpha_\infty}{dT} = 0$

$T_{ref} = 90\,C$

$WLF\ \ C_1 = 16$

$WLF\ \ C_2 = 57\,C$

$Clock\ \ C_3 = 1000$

$Clock\ \ C_4 = 51000$

$\beta_1 = 0.28$

$\tau_1 = 1\,sec$

These are
Volumetric CTEs

Relax Time (s)	Shear Prony Coef
0	1.0e-15
0	1.0e-14
0	1.0e-13
0	1.0e-12
0	1.0e-11
0	1.0e-10
0.0246248	1.0e-9
0.0176138	1.0e-8
0.0222504	1.0e-7
0.0351104	1.0e-6
0.046387	1.0e-5
0.0480215	1.0e-4
0.0807426	1.0e-3
0.00305496	5.0119e-3
0.13674	1.0e-2
0.21094	1.0e-1
0.173658	5.0119e-1
0.00768961	1.0e00
0.115825	1.9953e00
0.0405338	1.0e+1
0.0261315	5.0199e+1
0.00244998	1.0e+2
0.00239911	1.9953e+3
0	1.0e+4
0	1.0e+5
0.00582786	1.0e+6
0	1.0e+7
0	1.0e+8

DISTRIBUTION

1	MS0386	Jeff Lantz	02159
2	MS0481	Joe Fonseca	02224
3	MS0958	Mike Kelly	01833
4	MS0958	Jamie Kropka	01853
5	MS0888	Jim McElhanon	01853
6	MS0888	Ed Russick	01833
7	MS1411	Mat Celina	01853
8	MS0899	Technical Library	09536 (electronic copy)

Sandia National Laboratories